Variations in the aerosol optical properties and types over the tropical urban site of Hyderabad, India

D. G. Kaskaoutis,[1] K. V. S. Badarinath,[2] Shailesh Kumar Kharol,[2] Anu Rani Sharma,[2] and H. D. Kambezidis[1]

[1] Aerosol measurements over the tropical urban site of Hyderabad, India, provide a way of determining the variability of the aerosol characteristics over a duration of 1 year (October 2007 to September 2008). The meteorological pattern over India, mainly driven by the regional monsoons, has a great effect on the amount and size distribution of the aerosols. Higher aerosol optical depth (AOD) values are observed in premonsoon, while the variability of the Ångström exponent (α) seems to be more pronounced, with higher values in winter and premonsoon and lower values in the monsoon periods. The AOD at 500 nm (AOD_{500}) is very large over Hyderabad, varying from 0.46 ± 0.17 in postmonsoon to 0.65 ± 0.22 in premonsoon periods. A discrimination of the different aerosol types over Hyderabad is also attempted using values of AOD_{500} and $\alpha_{380-870}$. Such discrimination is rather difficult to interpret since a single aerosol type can partly be identified only under specific conditions (e.g., anthropogenic emissions, biomass burning or dust outbreaks), while the presence of mixed aerosols, without dominance of the coarse or accumulation mode, is the usual situation. According to the analysis the three individual components of differing origin, composition and optical characteristics are (1) an urban/industrial aerosol type composed of aerosols produced locally and all year round by combustion activities in the city or long-range transported (mainly in spring) biomass burning, (2) an aerosol type of mineral origin raised by the wind in the deserts (mainly in premonsoon) or constituting coarse-mode aerosols under high relative humidity conditions mainly in the monsoon period, and (3) an aerosol type with a marine influence under background conditions occurring in monsoon and postmonsoon periods. Nevertheless, the mixed or undetermined aerosol type dominates with percentages varying from 44.3% (premonsoon) to 72.9% (postmonsoon). Spectral AOD and α data are analyzed to obtain information about the adequacy of the simple use of the Ångström exponent for characterizing the aerosols. This is achieved by taking advantage of the spectral variation of $\ln AOD$ versus $\ln \lambda$, the so-called curvature. The results show that the spectral curvature can be effectively used as a tool for aerosol types discrimination, since the fine-mode aerosols exhibit negative curvature, while the coarse-mode particles are positive.

1. Introduction

[2] Aerosols play an important role in the Earth-atmosphere system and can affect general atmospheric circulation patterns [*Kristjànsson et al.*, 2005; *Lau et al.*, 2006] and biochemical cycling [*Xin et al.*, 2005]. However, there is

large uncertainty regarding the overall aerosol climatic effect [*Morgan et al.*, 2006; *Remer and Kaufman*, 2006; *Yu et al.*, 2006]. Because of the variety of aerosol sources, their short atmospheric lifetimes and the dynamic processes that may alter them after generation, their physical and chemical characteristics are highly inhomogeneous in space and time. Therefore, the accurate assessment of the aerosol impact on radiative transfer is a complex task, since various aerosol types cause different effects on the solar radiation spectral distribution [*Kaskaoutis and Kambezidis*, 2008a]. Indeed, a full description of all the characteristics that control aerosol interaction with solar and terrestrial radiation is needed. Better estimates of the aerosol radiative effects at a planetary

---

[1]Atmospheric Research Team, Institute for Environmental Research and Sustainable Development, National Observatory of Athens, Athens, Greece.
[2]Atmospheric Science Section, Oceanography Division, National Remote Sensing Centre, Department of Space, Government of India, Hyderabad, India.

scale are required to reduce the uncertainties. To achieve this, it is necessary to obtain a better characterization of the aerosol physical and optical properties [*McComiskey et al.*, 2008; *Tafuro et al.*, 2007]. To understand the effect of aerosols on the Earth-atmosphere system, it is essential to study and understand their physical, chemical, and optical properties [*Moorthy et al.*, 1999; *Satheesh et al.*, 2002]. Therefore, numerous studies have been undertaken to characterize the aerosol properties at several worldwide locations [*Dubovik et al.*, 2002; *Pace et al.*, 2006; *Kaskaoutis et al.*, 2007a; *El-Metwally et al.*, 2008; *Ogunjobi et al.*, 2008].

[3] The atmospheric aerosols may be of natural origin such as the windblown mineral dust or of anthropogenic origin such as those from industry, automobiles or other human activities in urban areas [*Kaskaoutis et al.*, 2007a]. They may originate from gas-phase reactions of low volatile vapors in the atmosphere [*Anttila et al.*, 2007]. The natural aerosols, due to their dominant share (80%), evidently play a vital role in global-scale climate, whereas the anthropogenic aerosols play crucial role in regional-scale climatic features [*Ramachandran*, 2004]. So, it is required to delineate the effects of natural and anthropogenic aerosols as far as regional features are concerned. *El-Metwally et al.* [2008] found that Cairo's aerosols are a mixture of three individual components produced by different mechanisms: local urban activities as "background pollution," biomass burning in the Nile delta as "pollution-like" and wind erosion in Sahara as "dust-like." Furthermore, *Pace et al.* [2006] found three individual aerosol types in Lampedusa, mainly consisting of European pollution, Atlantic clean marine and African dust particles.

[4] Aerosol mass burden and the extinction efficiency of aerosols are the most comprehensive variables to determine the AOD. From the spectral AOD, the Ångström formula [*Ångström*, 1964] is used in order to obtain the turbidity coefficient (β) and the wavelength exponent (α), which give information about the columnar burden and aerosol size, respectively. Recent research has forwarded to other related variables, such as the curvature of the spectral AOD (in the form of a lnAOD versus lnλ plot), which can be used to have some insight in the aerosol size distribution [*Eck et al.*, 1999; *Kaskaoutis et al.*, 2007b]. The curvature can be utilized in conjunction with the AOD for the discrimination of the different aerosol types, and can also be used as an indicator of the relative influence of fine- versus coarse-mode particles in the aerosol size distribution [*Schuster et al.*, 2006].

[5] India is densely populated, industrialized and in the recent years has witnessed an impressive economic development. Aerosols over and around India not only affect the Indian monsoon but also the global climate [*Satheesh et al.*, 2006]. The growing population coupled with revolution in industry has resulted in higher demands for energy and transport. With more and more urbanization the usage pattern of fossil and biofuels are leading to changes in aerosol properties, which may cause changes in precipitation and can decelerate the hydrological cycle [*Ramanathan et al.*, 2001]. Over urban areas of India aerosol emissions from fossil fuels such as coal, petrol and diesel oil dominate [*Habib et al.*, 2006]. Furthermore, the Indian subcontinent exhibits different land characteristics ranging from vegetated areas and forests to semiarid and arid environments and tall mountains. India experiences large seasonal climatic variations, which result in extreme temperatures, rainfall and relative humidity. These meteorological and climatic features introduce large variabilities in aerosol optical and physicochemical characteristics at spatial and temporal scales.

[6] The scope of this work is to analyze the results of Sun photometer measurements performed between 3 October 2007 and 30 September 2008 over the tropical urban site of Hyderabad, India. The AOD measurements performed by Microtops-II several times a day provide a unique opportunity for determining the temporal variability of aerosol characteristics. The 1-year measurements allow to characterize the seasonal pattern of aerosol properties, whose influence on the environment is thought to have an impact at least at regional scale. This seasonal pattern is expected to be important because (1) Hyderabad is a location where aerosols from different origins are mixed and in proportions that depend on the activity of their sources some of which are highly seasonal, (2) of the seasonal variation of the forest fires affecting the area [*Badarinath et al.*, 2007a, 2007c], and (3) of the specific seasonal meteorological pattern driven by the monsoons and the location of the Inter-Tropical Convergence Zone (ITCZ). Previous studies over Hyderabad were mainly focused on examining the variations in black carbon (BC) concentrations, AOD, UV index and solar radiation during short time intervals or under specific events, such as biomass burning or dust transport, by comparing the observations of "normal" and "polluted" days [*Latha and Badarinath*, 2005; *Badarinath et al.*, 2007b, 2007c, 2008, 2009]. The present study is among the first over Hyderabad focusing on the seasonal pattern of aerosol properties and types and aiming at associating them with local emissions, regional climatology and long-range transport.

2. Regional Characteristics, Meteorology, and Data Set

2.1. Site Description

[7] With its ~5.5 million inhabitants, Hyderabad (17.47° N, 78.43° E) is the fifth largest city in India, and is also considered as one of the most polluted [*Naseema Beegum et al.*, 2009]. This is a direct result of the growth in population and associated activities that have been observed during the last decades. In addition to this, particles produced by seasonal sources can be transported to Hyderabad at certain times of the year. This is the case of mineral dust produced mainly in premonsoon, though not exclusively, and the mass burning of the crop residues as well as forest fires in the dry period of the year. Because of its potential effects on people's health, the persistence of high levels of particulate concentrations and BC over Hyderabad [*Naseema Beegum et al.*, 2009] is a matter of great concern for its inhabitants. Accurate determination of the aerosol properties is necessary in order to quantify these effects.

2.2. Meteorology Patterns

[8] The well established linkage of dynamic and thermodynamic features, such as the setup of a low-level jet, warm pool and land-ocean thermal gradients influences forthcoming monsoonal features over the Indian subcontinent [*Lau et*
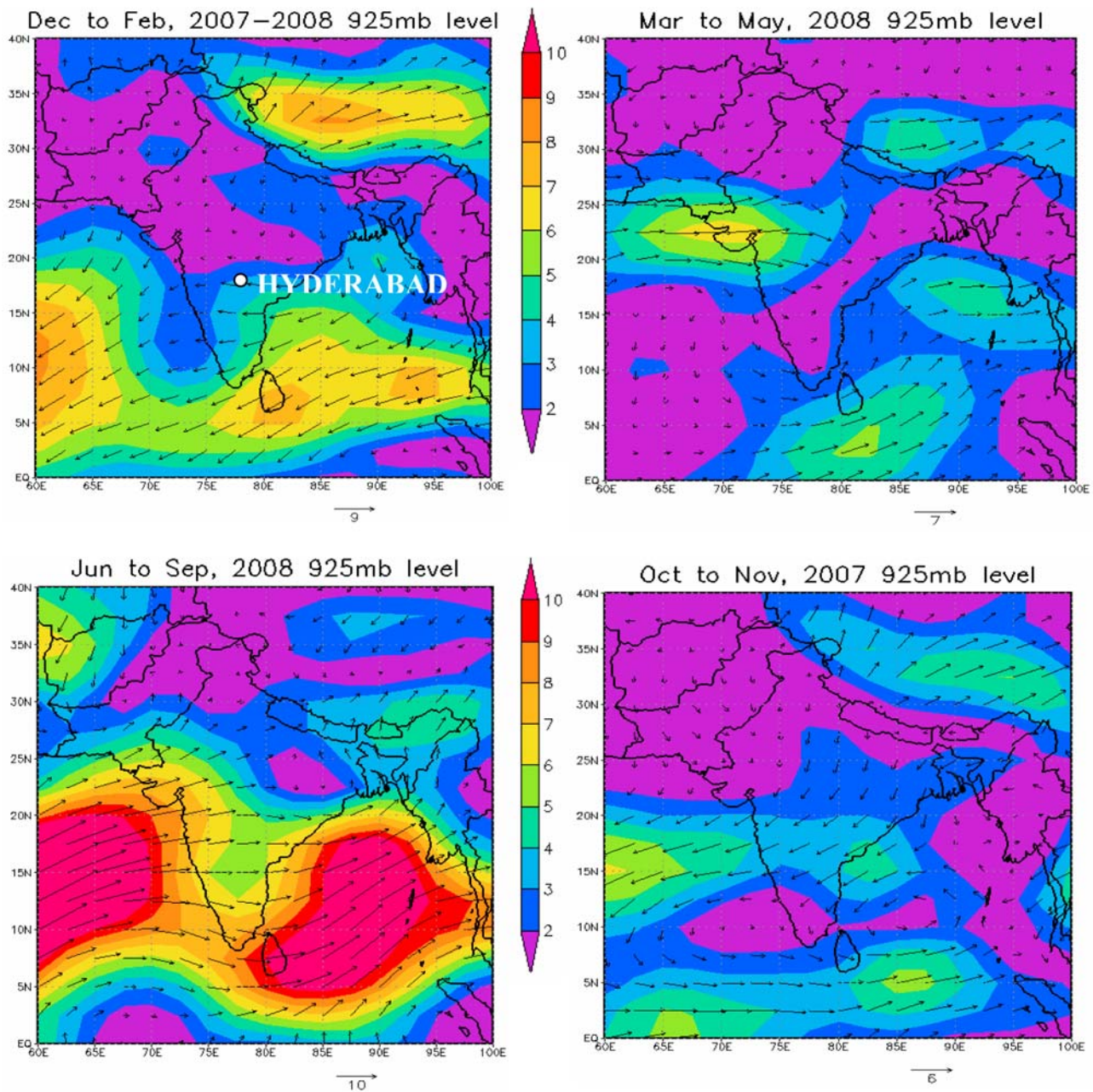
Figure 1. NCEP/NCAR reanalysis mean vector wind composites at 925 mbar level for winter (December–February), premonsoon (March–May), monsoon (June–September), and postmonsoon (October–November) seasons during the measurement period (3 October 2007 to 30 September 2008).

al., 2006]. Hence, besides the dynamic and thermodynamic linkage, the role of aerosols over India is also expected to play a critical role on monsoon features over the region [e.g., *Devara et al.*, 2003] and partly on global climate through the radiation budget.

[9] The mean composite vector wind at 925-mbar level over the Indian region is shown in Figure 1 for the four seasons considered. These maps were obtained from NCEP/ NCAR reanalysis and are the mean composites in each examined period, while the wind speed is shown in colored scale. In the winter, the winds over the Indian subcontinent are generally low, exhibiting larger speeds over the oceanic

areas. The wind flows mainly from eastern/northeastern directions, carrying significant amounts of polluted air masses over the Arabian Sea (AS) in certain cases. Fair weather conditions with clear skies exist during winter with continental air masses passing over the region [*Pandithurai et al.*, 2007]. Low-level inversions in the morning and evening hours, and haze in the morning occur during this period along with the incursion of dry polar continental air in the wake of low-pressure systems. In general, during premonsoon season (March–May), the weather over and around India is very hot with a daily maximum temperature around 40°C, while the surface winds are mostly gusty,

Table 1. Monthly Mean Values, as Well as Standard Deviations, of Several Meteorological Parameters at Hyderabad During the Period of Measurements, October 2007 to September 2008

Months	Temperature (°C)	Wind Speed (m s^{-1})	Wind Direction (degrees)	Pressure (mbar)	Relative Humidity	Rainfall (mm)
January	22.0 ± 4.4	1.2 ± 0.9	126.8 ± 74.9	948.4 ± 3.5	58.2 ± 23.8	0
February	24.1 ± 3.9	1.3 ± 0.9	117.8 ± 76.9	945.4 ± 2.5	60.0 ± 22.7	0
March	26.0 ± 4.0	1.2 ± 1.0	149.3 ± 75.8	946.7 ± 2.6	54.0 ± 23.3	0
April	30.0 ± 5.3	1.3 ± 0.9	191.1 ± 93.8	947.4 ± 2.9	45.7 ± 21.8	12.56
May	31.2 ± 4.2	2.3 ± 1.7	249.6 ± 60.8	945.1 ± 2.0	33.1 ± 13.7	0
June	27.7 ± 3.2	2.9 ± 1.2	233.9 ± 21.1	944.1 ± 1.7	59.2 ± 16.6	130.48
July	27.4 ± 2.8	2.3 ± 1.3	221.2 ± 56.8	943.4 ± 2.3	78.6 ± 16.5	97.94
August	25.0 ± 2.5	1.4 ± 1.3	255.7 ± 73.8	944.3 ± 2.7	85.3 ± 12.8	212.7
September	25.3 ± 2.9	1.8 ± 1.1	211.9 ± 65.7	945.2 ± 2.8	84.0 ± 14.3	264.1
October	23.7 ± 4.2	1.5 ± 1.1	136.4 ± 117.8	947.5 ± 3.1	67.5 ± 19.3	20.9
November	21.6 ± 5.3	1.5 ± 1.3	117.2 ± 117.1	950.4 ± 1.9	58.1 ± 23.0	20.9
December	21.8 ± 4.4	1.1 ± 0.9	134.4 ± 106.5	950.0 ± 3.1	61.0 ± 19.8	0

especially over northern AS, northern Indian Ocean (NIO) and Bay of Bengal (BoB). The dust content over northwestern India (Thar Desert) is at its maximum and often dust exposures affect Hyderabad, while cumulonimbus clouds develop around late afternoon to evening hours. Development of low-pressure systems due to increased heating over land start in premonsoon, when all India has the same pressure distribution, with only slightly higher pressure over the AS and the BoB [*Pandithurai et al.*, 2007]. The Indian summer monsoon (June–September) is a part of a large-scale circulation pattern, which develops in response to the thermal gradients between the warm Asian continent in the north and cooler NIO in the south. A strong southwesterly flow in the lower troposphere brings a substantial supply of moisture into India, which is released as precipitation almost across the entire country. In this period, the most strong and gusty winds occur all over the region. Monsoon and aerosol loading in the atmosphere are very intricately related to each other because of the amount and type of the aerosols, which act as cloud condensation nuclei (CCN), together with the available moisture in the atmosphere that determines the amount of rainfall occurring over the region. In the postmonsoon period (October–November 2007) a low-pressure system was developed over South India resulting in moderate winds from northeastern directions over AS and continental India, and in a persistent western flow over NIO.

[10] Table 1 shows the monthly mean values of ambient air temperature, wind speed and direction, atmospheric pressure, relative humidity (RH) and accumulated precipitation in the period October 2007 to September 2008 over Hyderabad. The air temperature is high varying from 22.0°C ± 4.4°C in January to 31.2°C ± 4.2°C in May. The surface-level wind follows variable directions, from southeasterly in the period October to March to southwesterly in the period April to September. The large standard deviations in each month, and especially in the period October–December, indicate the strong variability in wind direction within these months. Furthermore, the winds are generally low, enhanced in the monsoon period only. During this period the prevailing wind is southwesterly and the aerosols over Hyderabad have a possible influence of marine air masses reaching the region from AS and the Indian Ocean. In the premonsoon, the winds are predominantly westerlies and northwesterlies. The atmospheric

pressure shows lower values during the monsoon period. The RH exhibits high values, mainly in the monsoon period with monthly mean values above 80% (July to September). In March–May, also called dry season, the RH values are the lowest, and the dry and semiarid landscapes become the sources of mineral or desert dust. On the other hand, the dry weather and the absence of precipitation cause the favorable conditions for the occurrence and spread of forest fires. Precipitation is absent in winter and premonsoon, except April, while it is high in the monsoon months, with large rainfall amounts in August and September.

2.3. Sun Photometer Measurements

[11] The spectral AOD over the urban region of Hyderabad was measured at six wavelengths centered on 380, 440, 500, 675, 870 and 1020 nm using a handheld multichannel Sun photometer (Microtops-II). Previous studies using the Microtops-II showed a typical error in AOD measurements of ±0.03 [*Morys et al.*, 2001; *Porter et al.*, 2001; *Ichoku et al.*, 2002]. The full width at half maximum (FWHM) bandwidth at each of these wavelength channels is 2.4 ± 0.4 nm, and the accuracy of the Sun-targeting angle, i.e., field of view (FOV), is ∼2.5°. Great care has also been taken to avoid any error in sun targeting the Microtops-II by mounting the instrument on a tripod stand. Measurements of AODs with the same Microtops-II have been used in several studies by the same authors, while the overall procedure of retrieving spectral AOD from solar irradiance measurements is described by *Badarinath et al.* [2007c].

[12] The spectral AOD values were measured at 30-min intervals, from 0900 to 1700 local time (LT) on cloud-free skies. The AOD data was also subjected to cloud screening using the columnar water vapor values obtained from Sun photometer in addition to sudden departure in AOD values from the mean AOD values for the day. The changes of more than 3 standard deviations from the mean AOD were scrutinized for possible cloud contamination [*Smirnov et al.*, 2000]. The overall error in AOD [*Russell et al.*, 1993] can be due to the diffuse radiation entering the optical channel, the computational error in relative air mass, the deviation of the calibration coefficient with time and the error associated with the uncertainty in the optical depths owing to Rayleigh scattering and absorption by O_3, NO_2 and water vapor. The contribution of the latter errors in such high AOD values is very low though [*Kaskaoutis et al.*, 2007c]. The absolute

uncertainty in the AOD is about 0.03 with the larger values to be depicted at the shorter wavelengths and under low turbid conditions. Perturbed irradiance measurements from possible cloud contamination caused by undetected with naked eye cirrus clouds have been excluded if they conclude to AODs and Ångström exponent values up to two standard deviations from the mean daily value. After these procedures 3336 measurements remained for further analysis. Thus, depending on the sky conditions the number of available data are 1176 in the winter (December to February), 1080 in the premonsoon (March to May), 423 in the monsoon (June to September) and 657 in the postmonsoon (October–November) periods. It should be noted that during the monsoon months the intense cloud cover restricted the number of days for AOD retrievals, since the Microtops-II was not operated during cloud passage. The cloud contamination may also have an influence on the lower Ångström's exponent values in this period.

3. Data Analysis and Methodology

[13] The spectral dependence of AOD is used in this work to compute the Ångström's exponent α. A spectrally averaged value of this exponent, which contains information about the size of the particles or the volume fraction of the fine- versus coarse-mode particles [*Schuster et al.*, 2006], can be obtained by fitting the Ångström's formula [*Ångström*, 1964]:

$$AOD_\lambda = \beta \lambda^{-\alpha}, \tag{1}$$

where AOD_λ is the estimated AOD at the wavelength λ, β is the Ångström's turbidity coefficient, which equals AOD at $\lambda = 1\ \mu m$, and α is the Ångström exponent. Although in this definition α is assumed independent to the wavelength, it is well known that depends on it [*Kaskaoutis and Kambezidis*, 2008b, and references therein]. The Ångström formula is a special case of a more complicated equation valid for a limited range of particle diameters and a limited interval of wavelengths. The validity of this theory presupposes that the Junge power law is valid for the particle radius range, where significant extinction takes place and that the spectral variation of the refractive index does not impose significant variations on the Mie extinction factor [*Kaskaoutis et al.*, 2006]. Taking the logarithms at both sides of equation (1) one obtains

$$\ln AOD_\lambda = -\alpha \ln \lambda + \ln \beta. \tag{2}$$

A more precise empirical relationship between aerosol extinction and wavelength is obtained with a second-order polynomial approximation [*King and Byrne*, 1976; *Eck et al.*, 1999; *Pedrós et al.*, 2003; *Kaskaoutis and Kambezidis*, 2006],

$$\ln AOD_\lambda = a_2 (\ln \lambda)^2 + a_1 \ln \lambda + a_o, \tag{3}$$

where the coefficient a_2 accounts for a curvature often observed in Sun photometry measurements. This curvature can be an indicator of the aerosol particle size, with negative curvature indicating aerosol size distributions dominated by fine-mode and positive curvature indicating size distributions with significant contribution by the coarse-mode aerosols [*Eck et al.*, 1999; *Schuster et al.*, 2006]. In this study, the values of α were computed in the wavelength interval 380–870 nm, applying the least squares method to equation (2). The linear fit to the logarithmic function of equation (2) is the most precise method, although the results may also depend on the spectral interval considered [*Pedrós et al.*, 2003]. The second-order polynomial fit (equation (3)) was also applied to the AOD values at five wavelengths (380, 440, 500, 675 and 870 nm). Although the polynomial fit to equation (3) is more precise than the linear fit to equation (2), large errors can appear especially under low-turbidity conditions [*Kaskaoutis et al.*, 2006]. For limiting these errors, only the cases where the second-order polynomial fit was associated with $R^2 > 0.95$ were considered. It should be noted that the AOD_{1020} values were omitted from the fits, since they contain larger uncertainties due to the water-vapor effect and detector temperature sensitivity.

[14] As atmospheric aerosols are highly heterogeneous, no single technique or group of techniques is absolutely adequate for an entire characterization of the atmospheric aerosol properties over the extremely wide range of particle sizes, shapes and chemical compositions, or to classify them into groups or types [*El-Metwally et al.*, 2008]. The selection of a particular method depends primarily on the type of application. In the case of atmospheric aerosols monitored by Sun photometers, the columnar mass concentration and the size distribution are vital to understand their source region and optical properties; the first is parameterized by the spectral AOD, while the latter via the Ångström's exponent. Possible correlations linking AOD to α can be sought by examining the scatterplot of α versus AOD. As detailed by several studies [e.g., *Pace et al.*, 2006; *Kaskaoutis et al.*, 2007a; *El-Metwally et al.*, 2008], this visual representation often allows one to define physically interpretable cluster regions for different types of aerosols with different optical characteristics. The importance of these properties is also high for atmospheric and remote sensing studies, apart from other research fields. All these emphasize the need for extensive measurements and analysis of the aerosol optical properties at as many locations on Earth as possible.

[15] In such studies, the selection of the threshold values for the distinguish of the aerosol types can be very important. Therefore, in the present work, the threshold values must be different from those utilized by previous studies, for example, *Pace et al.* [2006] for Lampedusa, *Kaskaoutis et al.* [2007a] for four AERONET sites, *Kaskaoutis et al.* [2007d] for Athens and *El-Metwally et al.* [2008] for Cairo, directly modulated by the specific characteristics of each location. Since Hyderabad is a densely populated and highly industrialized area, the AOD_{500}, even on days without pollution is rather high, $\sim 0.35-0.45$ [*Latha and Badarinath*, 2005; *Badarinath et al.*, 2009]. Furthermore, the AOD_{500} can be above 0.5 during biomass burning conditions [*Badarinath et al.*, 2007c] or >0.6 under the influence of dust plumes [*Badarinath et al.*, 2007a]. Therefore, (1) values of $AOD_{500} < 0.3$ with $\alpha_{380-870} < 0.9$ represent background conditions with a marine influence, thus corresponding to a Marine Influenced (MI) aerosol
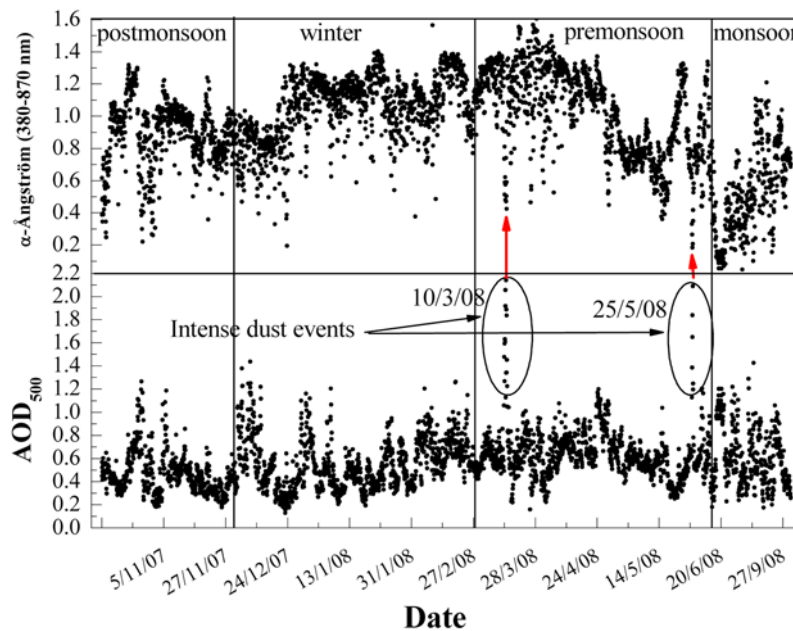
Figure 2. Variation of AOD_{500} and $\alpha_{380-870}$ over Hyderabad during the period of measurements (3 October 2007 to 30 September 2008).

type; (2) $AOD_{500} > 0.5$ and $\alpha_{380-870} > 1.0$ can be used to characterize urban/industrial aerosols under High AOD (HUI), also including the biomass burning episodes, and (3) $AOD_{500} > 0.6$ associated with $\alpha_{380-870} < 0.7$ are indicative of desert dust particles under High AOD (HDD). Finally, the remaining cases, not belonging in any of the above groups, are characterized as mixed type (MT) or undetermined aerosols [*Pace et al.*, 2006]. In the present work a higher AOD_{500} threshold value is used from the aforementioned studies for the characterization of the MI conditions, since the AOD_{500} is relatively large over Hyderabad even on "normal" days (i.e., days with background air pollution levels, e.g., traffic and domestic pollution). A lower threshold $\alpha_{380-870}$ value for the characterization of the HUI aerosols was selected since the available data set was taken over a location far away from areas directly affected by fresh smoke of biomass burning and the Ångström exponent of pollution may be lower due to hygroscopic growth of fine anthropogenic water-soluble particles into larger accumulation mode size [*Eck et al.*, 2005]. The $\alpha_{380-870}$ threshold value of 0.7 for characterizing desert dust aerosols was adopted here slightly higher than that (0.5) of *Kaskaoutis et al.* [2007a] since the desert particles transported over Hyderabad can be mixed with other aerosols (mainly anthropogenic) or to be deposited near the source region. However, because the exact value of α depends significantly on the spectral range used in its determination, the information contained in the $\alpha_{380-870}$ versus AOD_{500} scatterplots may be difficult to interpret.

4. Results and Discussion

4.1. Seasonal and Monthly Variations

[16] Figure 2 shows the fluctuation of all AOD_{500} and $\alpha_{380-870}$ observations during the study period. The results reveal significant day-to-day variability in both AOD_{500} and

$\alpha_{380-870}$, underlying the influence of varying aerosol types. In the postmonsoon and winter seasons (October to February) the AOD_{500} peaks are depicted on certain days, while in the premonsoon and monsoon periods (March to September) they are more often. Similarly, the $\alpha_{380-870}$ values are, in general, higher than 1.0 in the winter and premonsoon periods, while they significantly drop in monsoon. In Figure 2, two AOD_{500} peaks are depicted caused by very intense dust events that occurred on 10 March and 25 May 2008. Note that on these days the $\alpha_{380-870}$ present very low values. On the other hand, the increase in fine-mode particles loading due to long-range transport of aerosols from biomass burning is reflected in an increase of AOD and α. Such high values in AOD and α during forest fires have also reported over Hyderabad [*Kharol and Badarinath*, 2006; *Badarinath et al.*, 2009]. Aerosol properties over Hyderabad can be significantly modified by the advection of aerosols from the adjoining landmasses under favorable wind conditions [*Badarinath et al.*, 2007b, 2009]. Another possibility is that the increased convective turbulence during premonsoon months would be pumping in more surface-level aerosols to higher altitudes, which would decrease in the nighttime because of their tripped in the boundary layer height. In addition to this, the desert dust aerosols, advected by the westerly winds, would also contribute to increased coarse particle abundance.

[17] Figure 3 shows the monthly mean variation of AOD_{500} and $\alpha_{380-870}$ in the period October 2007 to September 2008. The vertical bars express 1 standard deviation, while the total number of data in each month is also given. Figure 3 reveals a rather insignificant monthly variation in AOD_{500}, from ~0.5 to ~0.7, with lower values in the October–January period and higher in the March–July one. In sharp contrast, the $\alpha_{380-870}$ values show a pronounced decrease in monsoon period (June to September). This strong decrease in $\alpha_{380-870}$ values may partly be
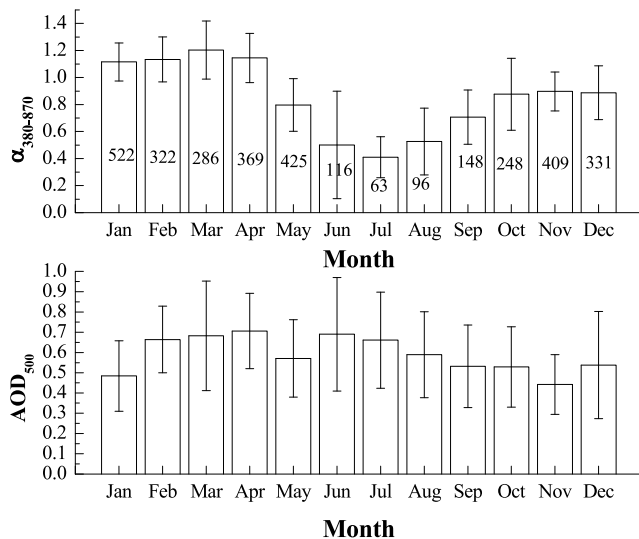
Figure 3. Monthly mean AOD_{500} and $\alpha_{380-870}$ over Hyderabad. The vertical bars denote 1 standard deviation, while the number of the measurements in each month is given within the bars of the top graph.

attributed to cloud contamination in the retrievals caused by thin undetected cirrus clouds. The largest monthly mean AOD_{500} in March and April are associated with large $\alpha_{380-870}$ values indicative of fine-mode particles. A possible explanation for this can lie on the fact that this is the time with peaks in forest fires in central and northern India [*Badarinath et al.*, 2007a] and the transport of biomass burning plumes toward Hyderabad by northerly winds (see Figure 9). Moreover, biomass burning aerosols may be produced by the burning of the vegetal residues in premonsoon, before the rains of the monsoon season. The contribution of biomass burning to the overall atmospheric load in BC over India can then increase from 30% [*Novakov et al.*, 2000] to 70% [*Alfaro et al.*, 2003] between the beginning and the end of March.

[18] Monthly variations in the aerosol size and its influence on AOD are clearly seen over Hyderabad. Coarse-mode and/or growth of fine-mode water-soluble (e.g., sulfate) aerosols due to higher ambient RH result in high AOD_{500} in the summer monsoon, while during the winter the AOD_{500} is slightly lower, which is mostly associated with fine-mode particles. Thus, it is observed that in the urban area of Hyderabad anthropogenic sources dominate the aerosol distribution, which could get modulated by the presence of natural aerosols. During monsoon the $\alpha_{380-870}$ values are being mediated by the higher ambient RH, possible cloud contamination and transport of dust and sea salt in favorable wind conditions. The high values of BC during the winter months have been attributed to the decreased boundary layer height causing low ventilation for mixing the emissions from vehicular traffic [*Latha et al.*, 2004; *Badarinath et al.*, 2007c]. However, *Badarinath et al.* [2007a] found large daily, monthly and annual variabilities in BC concentrations and aerosol size distribution (nucleation, accumulation and coarse particles), mainly driven by the fire events in the upwind regions adjoining to Hyderabad. Nevertheless, a slight reduction in AOD_{500} is

observed during the monsoon (August–September) due to scavenging effects of rainfall. On the other hand, high AODs during the premonsoon period could be attributed to the increased concentration of continental aerosols due to strong surface winds, which play an important role in lifting the loose soil, as well as other sources such as long-range transport of dust from northwestern India [*Badarinath et al.*, 2007b] or biomass burning since India experiences severe forest fires during January to May each year [*Badarinath et al.*, 2007a; *Kharol and Badarinath*, 2006]. The AOD values and their seasonal pattern over Hyderabad are similar to those presented over four (Chennai, New Delhi, Mumbai and Kolkata) Indian sites [*Ramachandran*, 2007].

[19] Figure 4 shows the frequency of occurrence of AOD_{500} for the four individual seasons. Large changes in the AOD_{500} values are observed in each season. In the winter a higher frequency is observed for AOD_{500} between 0.3 and 0.5. A rather similar distribution is shown in the monsoon period, which shows a higher frequency for larger AOD_{500} values. An almost normal distribution occurs, though, in the premonsoon. The AOD_{500} ranges between 0.1 and 1.2 in postmonsoon, where the highest frequency is observed for AOD_{500} values in the range 0.3–0.5. In each season the mean AOD_{500} values are also given for a direct comparison with the results from other Indian or worldwide urban areas. The cumulative frequency of observing an $AOD_{500} > 0.7$ is high (22.7% in winter, 30.4% in premonsoon, 30.1% in monsoon and 8.5% in postmonsoon) while values larger than 1.0 have also been recorded. This important frequency of occurrence for large AOD_{500} values confirms that the atmospheric load over Hyderabad is usually particularly high. These large AODs are in the same order of magnitude with those presented over Cairo [*El-Metwally et al.*, 2008] and Kanpur [*Tripathi et al.*, 2005] and significantly higher that those at several urban AERONET locations [*Holben et al.*, 2001]. As expected, the aerosol load over Hyderabad is found to be much higher than that observed over the oceanic regions surrounding the Indian subcontinent, i.e., BoB (AOD_{500} = 0.36 ± 0.12), AS (AOD_{500} = 0.23 ± 0.09) and NIO (AOD_{500} = 0.26 ± 0.10), mean and standard deviations during the ICARB campaign [*Kalapureddy and Devara*, 2008]. The 5-year mean AOD_{550} is 0.4 in Chennai and Mumbai, while in Kolkata and New Delhi it is >0.55 [*Ramachandran*, 2007]. The mean AOD_{500} and Ångström exponent at Visakhapatnam, a costal urban area in BoB, were found to be 0.72 ± 0.39 and 0.88 ± 0.39, respectively in the period May–August 2005 [*Madhavan et al.*, 2008]. The mean AOD_{500} in the premonsoon season in Pune is 0.42, while in the winter ~0.38 [*Pandithurai et al.*, 2007]. These values are significantly lower than those over Hyderabad in the same periods, since Pune is not so industrialized and with much less population than Hyderabad.

[20] The frequency distribution of $\alpha_{380-870}$ (Figure 5) in all seasons reveals a great dispersion of the values thus denoting variability in the aerosol size distribution. Moreover, the frequency distribution is very different depending on season. In winter the $\alpha_{380-870}$ values are skewed toward larger values, while in monsoon toward lower. During winter, the modal value is around 1.2, indicating the dominance of submicron aerosols originating from biofuel
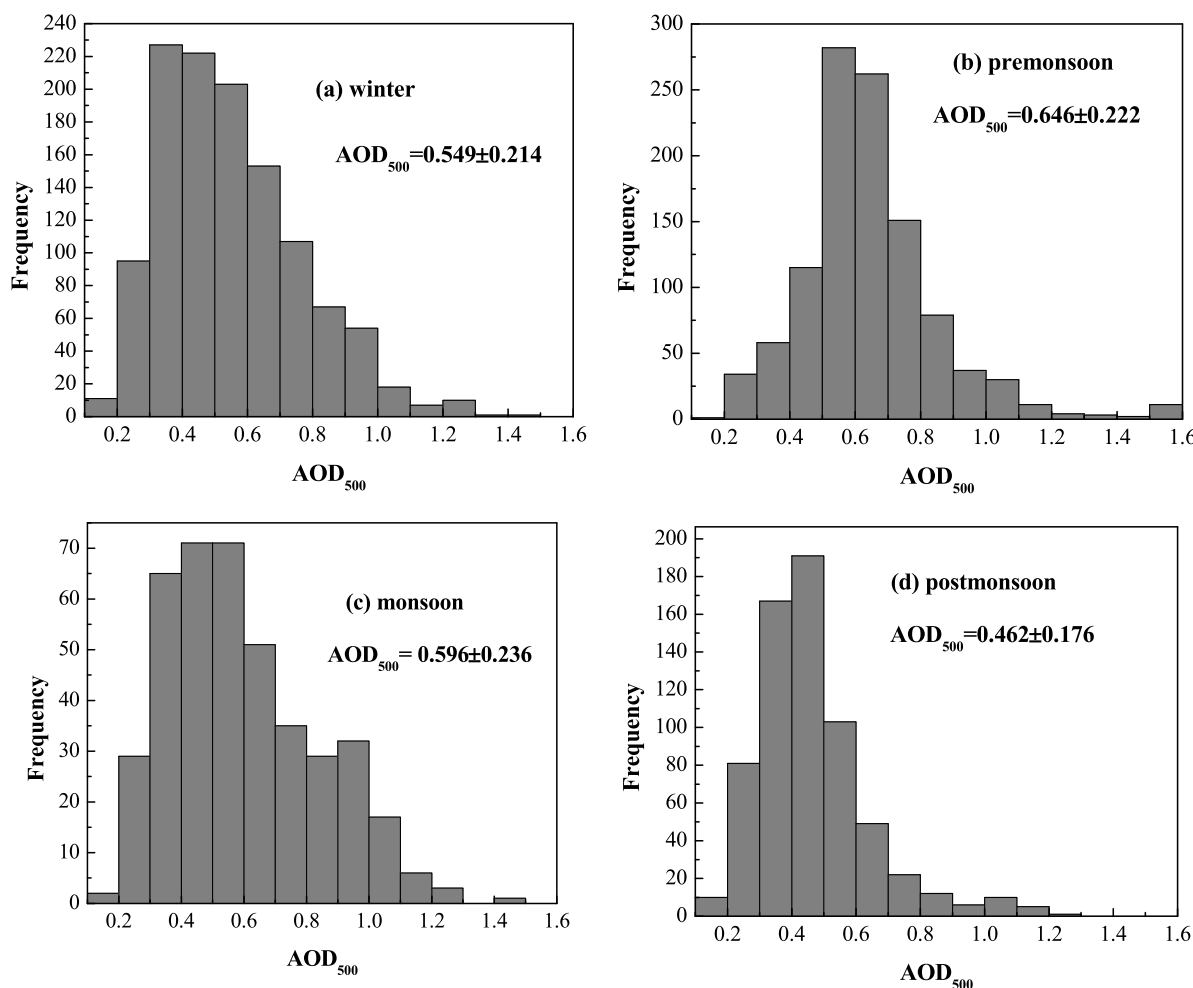
Figure 4. Frequency distribution of the AOD_{500} values in each season over Hyderabad during the period 3 October 2007 to 30 September 2008: (a) winter (December–February), (b) premonsoon (March–May), (c) monsoon (June–September), and (d) postmonsoon (October–November). The mean seasonal values are also given.

burning and fossil fuel combustion sources mainly. Moreover, the fact that $\alpha_{380-870}$ becomes less than 0.5 only rarely in winter shows that the influence of the dust aerosols is very limited. The dominating aerosols are in the submicron size range formed in situ by secondary gas-to-particle conversion processes of the precursors [*Badarinath et al.*, 2007a]. Moreover, the surface inversion associated with the trapping of pollutants give rise to hazy and foggy conditions [*Madhavan et al.*, 2008]. During premonsoon, $\alpha_{380-870}$ exhibits two modal values around 0.7 and 1.3, ranging from very low (<0.2) to very high (>1.5) values. This clearly indicates that the aerosol scenario over Hyderabad is driven by a combination of pollution and dust patterns due to dust generation from strong surface heating and high winds, as was also shown in Bahrein [*Smirnov et al.*, 2002]. Water-soluble aerosol particles (e.g., ammonium, nitrate, chloride and sulphate) mainly coming from industries and anthropogenic activities play a major role in the nucleation and growth of cloud droplets [*Roberts et al.*, 2002] especially in the monsoon season when RH is very high. The water uptake of such aerosols due to their hygroscopic nature results in size enlargement [*Day and Malm*, 2001] due to the humidification processes. This fact results in the

significantly lower $\alpha_{380-870}$ values observed in this season, which are partly attributed to the long-range transport of desert dust particles. In postmonsoon, the possibility of high (>1.1) and low (<0.6) $\alpha_{380-870}$ values is similar with higher frequency in the 0.9–1.0 interval. Values of $\alpha_{380-870} > 1.0$ are observed at 65.9% in the winter, 57.3% in premonsoon, 29.2% in postmonsoon and only 8.5% in the monsoon period and are typical of particles located mostly in the submicron range. On the other hand, values smaller than 0.5, and typical of aerosols containing an important proportion of particles larger than 1 μm [*Ångström*, 1964], are 0.9%, 2.3%, 43.4% and 5.5% in winter, premonsoon, monsoon and postmonsoon seasons, respectively. In Figure 5, the seasonal mean $\alpha_{380-870}$ values are also given. The large variability in aerosol size around India was established by *Kalapureddy and Devara* [2008] who found that the portion of $\alpha_{340-1020} < 1$ constitutes 2.6%, 37.3% and 74.6% of the total observations over BoB, NIO and AS, respectively. Thus, dominance of fine-mode ($\alpha = 1.21 \pm 0.11$) and coarse-mode ($\alpha = 0.86 \pm 0.20$) aerosol particles has been observed over BoB and AS regions, respectively.
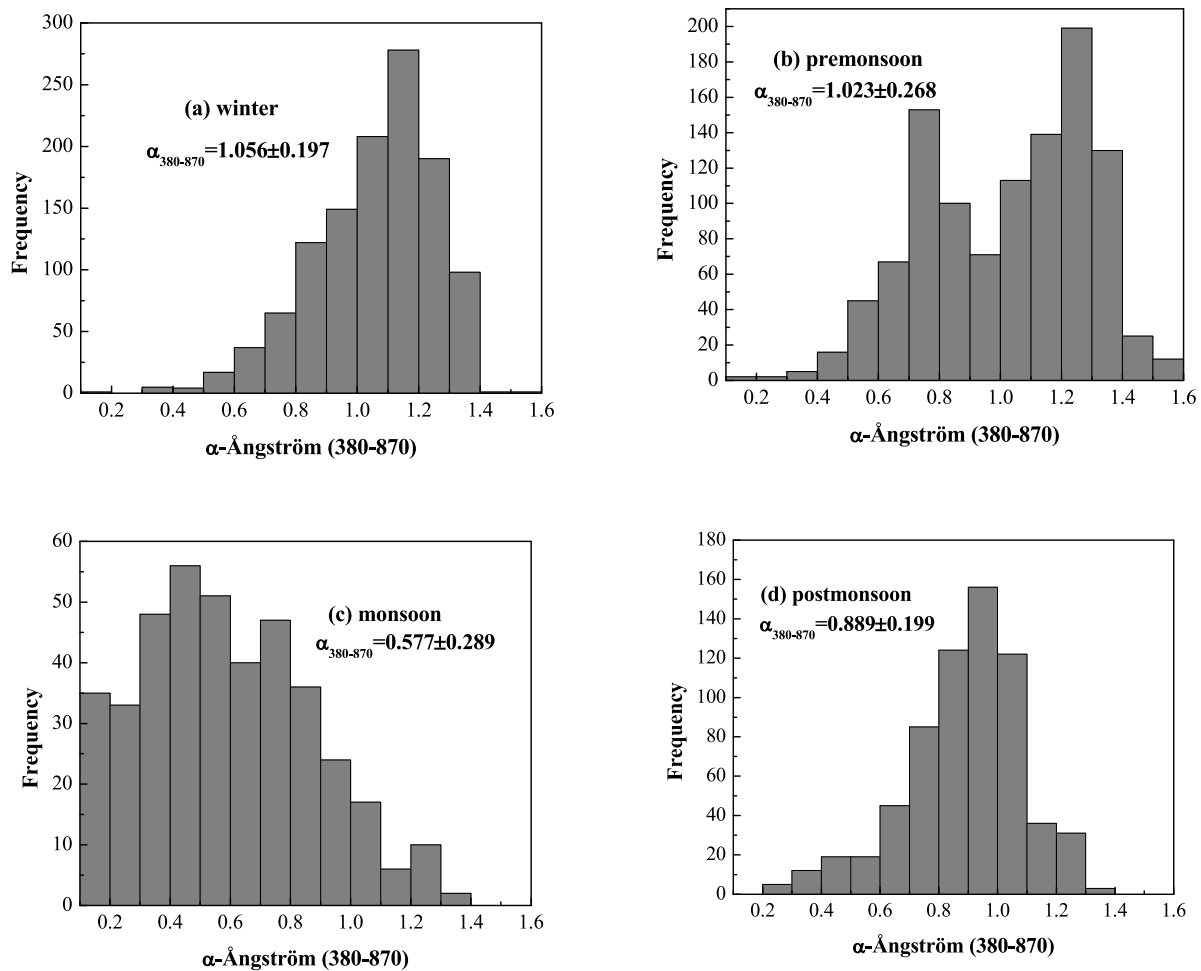
Figure 5. Same as in Figure 4 but for the $\alpha_{380-870}$ values.

4.2. Seasonal Discrimination of the Aerosol Types

[21] Figure 6 shows the density plot of AOD_{500} versus $\alpha_{380-870}$ over Hyderabad for the four individual seasons. These contour maps were constructed using a step of 0.1 for both AOD_{500} and $\alpha_{380-870}$ values. The white gaps correspond to lack of data. A striking feature of the scatterplot obtained is that a wide range of $\alpha_{380-870}$ is associated with values of $AOD_{500} < 0.4$. This indicates that under these conditions the aerosols are probably a mixture of several components differing in size and that the proportion of this mixture depends on season. The assumption that the aerosols over Hyderabad are of differing origins and optical properties is further supported by the fact that the large AOD_{500} are associated with narrow ranges of $\alpha_{380-870}$. However, the majority of the points in the scatterplots are confined by intermediate AOD_{500} and $\alpha_{380-870}$ values corresponding to a rather undetermined aerosol type, making thus the further characterization of the aerosols difficult, because of the complex combination of natural and anthropogenic factors (including RH, fuel types and emission characteristics) that influence aerosol formation and evolution.

[22] Viewing the contour plot some areas of larger density are observed, representative of different aerosol types depending on season. In winter, the maximum density area of ($AOD_{500} = 0.4-0.5$ and $\alpha_{380-870} = 1.1-1.2$) is representative of the urban polluted aerosols under moderate-to-high turbid conditions. The other $AOD_{500}/\alpha_{380-870}$ pairs are nearly equally distributed around this area with preferable of larger AOD_{500}. In the premonsoon season, the winter maximum seems to shift into two; one with $AOD_{500} = 0.5-0.7$ and $\alpha_{380-870} = 1.1-1.3$ with anthropogenic or biomass burning origin probably, and a second with $AOD_{500} = 0.5-0.6$ and $\alpha_{380-870} = 0.7-0.8$ corresponding to aerosols with larger fraction of coarse-mode particles under turbid conditions. In monsoon, the $\alpha_{380-870}$ values are significantly lower than those in the previous cases, mainly affected by the density maximum area of AOD_{500} ~ 1.0, $\alpha_{380-870}$ ~ 0.1. The different aerosol sources have a direct effect on the wide range of $\alpha_{380-870}$ values, from ~ 0.3 to ~ 1.0, especially for low AOD_{500} (<0.4), suggesting a range of aerosol types. However, for larger AOD_{500} the $\alpha_{380-870}$ decreases to values lower than 0.4, assigning a decreasing trend of the AOD_{500} versus $\alpha_{380-870}$ relationship. The postmonsoon is characterized by lower AOD_{500} (0.46 ± 0.18) and moderate $\alpha_{380-870}$ (0.89 ± 0.19) values. The maximum density area is observed for the pair (AOD_{500}, $\alpha_{380-870}$) = ($0.35-0.45$, $0.9-1.0$) indicative of
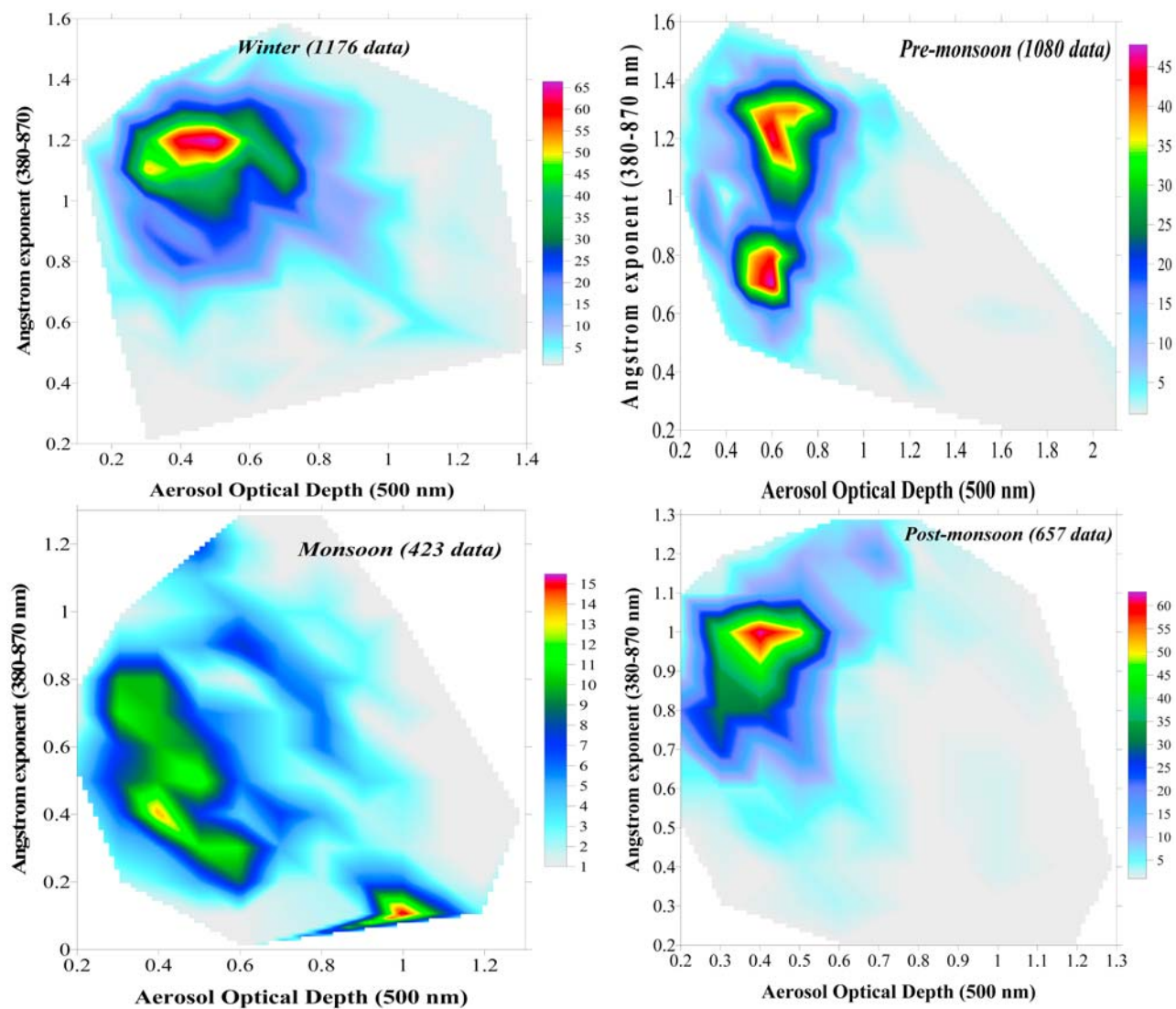
Figure 6. AOD_{500} versus $\alpha_{380-870}$ for each season during the period 3 October 2007 to 30 September 2008. The number of observations is shown in parentheses for each individual season.

moderately turbid conditions with a rather mixed aerosol field in the vertical. The α values of this magnitude are indicative of bimodal aerosol size distributions, with significant contribution from both fine-mode submicron (radius < 1 μm) and coarse-mode supermicron (radius > 1 μm) aerosols [*Eck et al.*, 2005].

[23] Figure 7 shows the percent contribution of each of the three different aerosol types over Hyderabad, based on the present AOD and $\alpha_{380-870}$ threshold values. It is observed that the MT aerosol is the most dominant contributor with varying magnitudes depending on season. The respective influences of the three aerosol types are more balanced in the winter and postmonsoon than during premonsoon and monsoon periods, when the % contribution of the specific aerosol types is larger. The contribution of aerosols of different origin and characteristics to the atmospheric column can be strongly modified in each season. Thus, 47.2% of the HUI aerosols are observed in premonsoon, 30.3% of HDD aerosols in monsoon and 8.7% of the

MI conditions in the postmonsoon periods. The MT is predominant in all seasons, except the premonsoon, exhibiting its higher frequency in postmonsoon (72.9%) and winter (62.2%). Quite characteristic is the low percentage of HUI aerosols in monsoon (6.6%), taking into account that the anthropogenic emissions are significant at Hyderabad throughout the year. This can partly be explained by a quick modification of the produced water-soluble local aerosols that can enlarge in size due to humidification especially under the influence of the large RH values in the summer monsoon. Also, significant role may play the dust emissions and transport in this season and the possible adhering of fine-mode pollution particles onto the surface of coarse-mode dust in the mixed aerosol. Since the majority of the aerosols belong to a mixed (or undetermined) aerosol type more attention must be paid to this type, as a result of independent processes. Thus, the mixing could be caused by primary small and large particles. The larger RH values close associated with the lower $\alpha_{380-870}$ in monsoon may
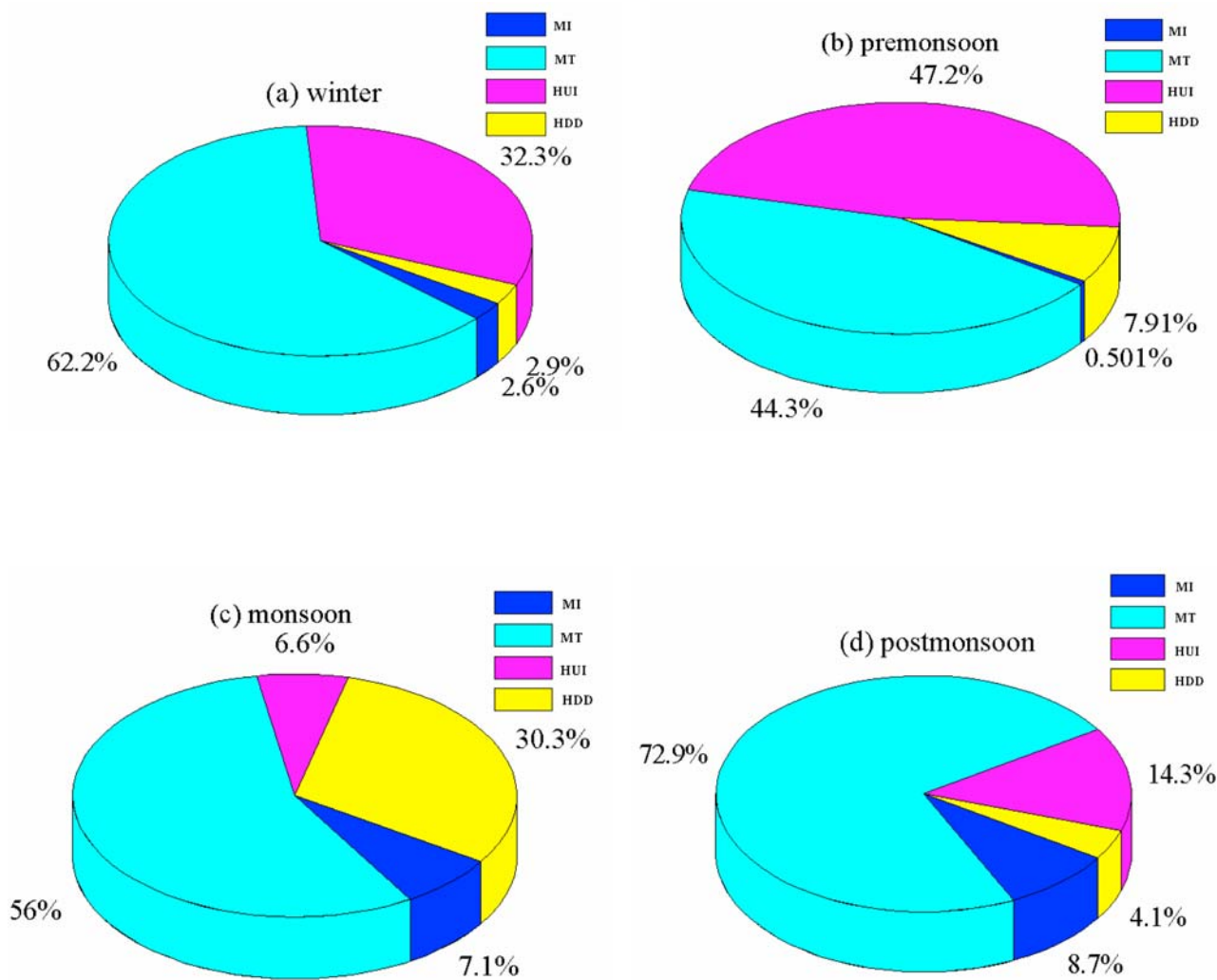
Figure 7. Fraction pies of each aerosol type over Hyderabad contributing to the total in each season: MI (maritime influenced), MT (mixed type), HUI (high AOD urban/industrial), and HDD (high AOD desert dust) for (a) winter, (b) premonsoon, (c) monsoon, and (d) postmonsoon.

be an evidence of coagulation and hygroscopic growth of the water-soluble urban aerosols, since the higher growth factor includes the hygroscopic and water-soluble particles [*Day and Malm*, 2001]. However, there is not a detailed analysis in the present study to warrant it and further investigation is needed. Also, the possible cloud contamination in some cases in the monsoon period results in lower $\alpha_{380-870}$, which associated with the high AODs concludes to the HDD type. On the other hand, the coarse-mode particles transported over Hyderabad can easily be mixed with local pollution or with smoke from forest fires, increasing the AOD wavelength dependence.

[24] Figure 8 shows the percentage frequency of occurrence for each aerosol type as a function of month. In particular, MT was observed in the whole duration of the measurements period. Thus, in certain months, the MT aerosols corresponded to more than 60% of the daily observations. Besides this fact, the dominance of the HUI aerosols is seen during the February–April period. Rice-crop residues are usually burnt in the Indo-Gangetic Plains
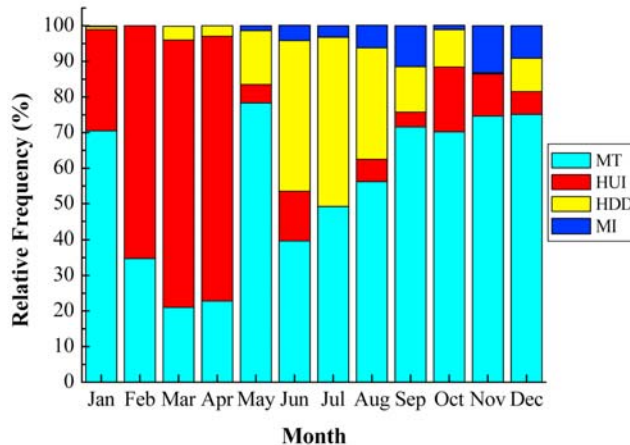

Figure 8. Relative (%) frequency of each aerosol type over Hyderabad for each month: MI (maritime influenced), MT (mixed type), HUI (high AOD urban/industrial), and HDD (high AOD desert dust).
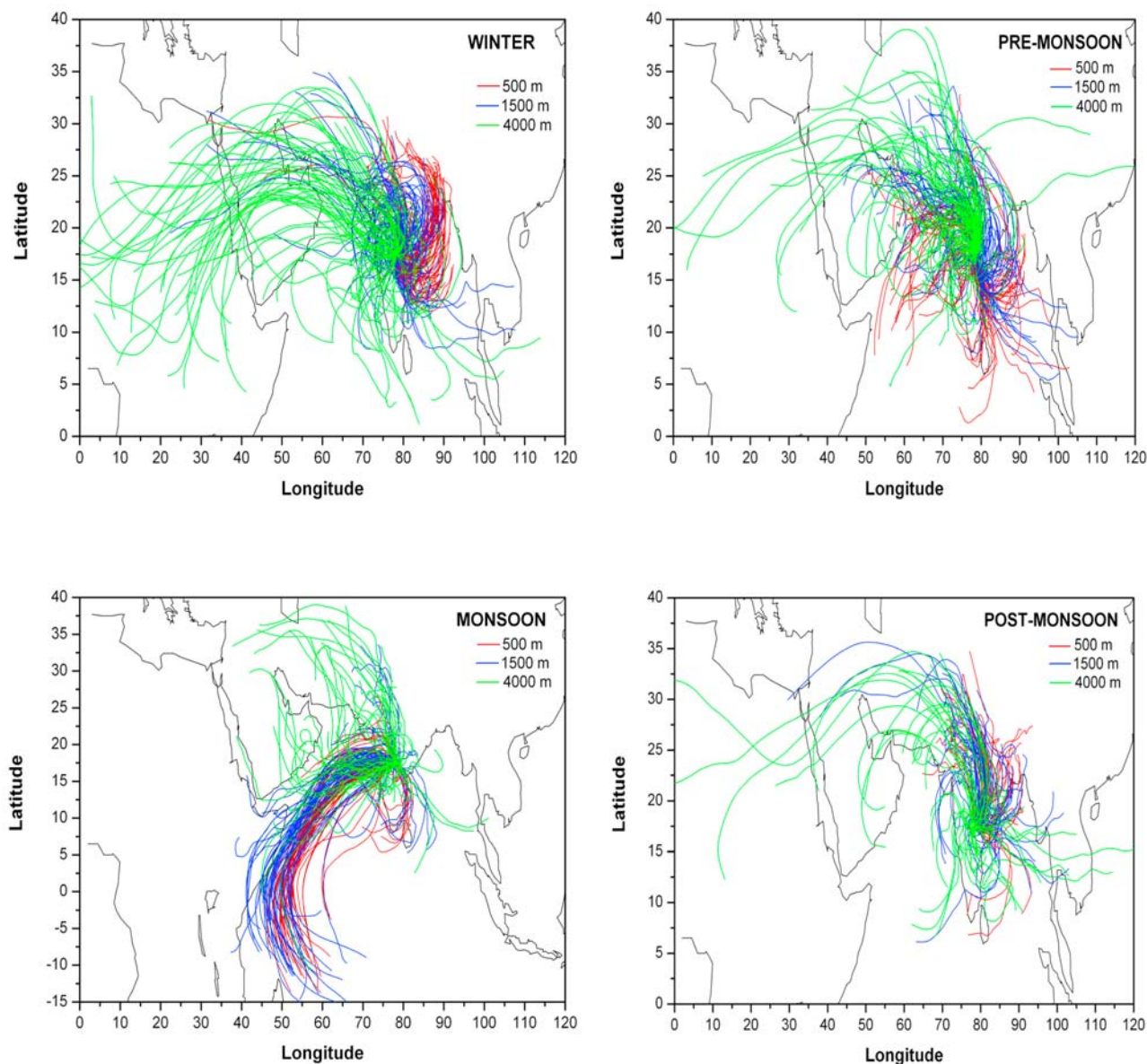
Figure 9. Five-day back trajectories ending at Hyderabad in each season at 500 m (red), 1500 m (blue), and 4000 m (green). The trajectories were taken from the HYSPLIT model and refer to 1000 UTC.

(IGP) during October/November each year. This large-scale burning constitutes a major source of submicron-sized aerosols, which are known to aggravate lung and respiratory diseases [*Wang and Christopher*, 2003] and affect Hyderabad on specific days of this period [*Badarinath et al.*, 2009]. The MI conditions show their largest fraction, although very small, from September to December, while HDD makes it's largest contribution in the period May to September.

4.3. Back Trajectory Analysis

[25] The aerosol load and types at any location are generally influenced by the meteorological conditions (primarily wind and convection) and hence affect the air mass transport over the region for a particular period. Figure 9 shows the 5-day back trajectories of NOAA-HYSPLIT

(National Oceanic and Atmospheric Administration Hybrid Single-Particle Lagrangian Integrated Trajectory) version 4 [*Draxler and Rolph*, 2003] model, where different types of air masses that influence AOD over Hyderabad are revealed in each season. The air masses are computed at three altitudes (500, 1500 and 4000 m) on each day with at least 3 AOD observations at 1000 UTC.

[26] In winter, there is a well-established difference between the pathways of the air masses at each altitude; thus, as the altitude increases the air mass source regions shift toward western directions. At 500 m the air masses come from northern/northeastern directions originating from Bangladesh and traversing the eastern Indian coast, where densely populated areas and industries are situated. At 1500 m the air masses are of continental origin, northern India and IGP, where often intense fog and pollution-haze
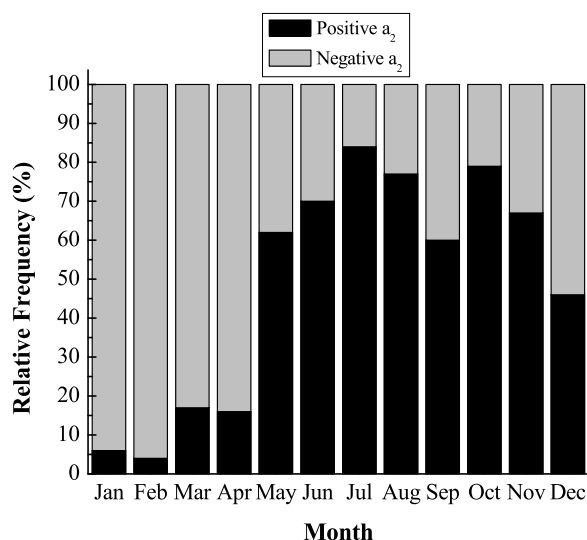
Figure 10. Frequency of occurrence (%) for the positive and negative a_2 values obtained from equation (3) for each season over Hyderabad.

conditions occur [*Badarinath et al.*, 2007a]. The lower altitude trajectories favor the transport of pollution aerosols over Hyderabad in winter; thus the relative high AODs compared with those from other urban locations (e.g., Athens, Cairo) in this season [*Kaskaoutis et al.*, 2007d; *El-Metwally et al.*, 2008]. At 4000 m the trajectories are from western directions, originating mainly from Africa and driven by the western synoptic circulation pattern in northern midlatitudes. However, the low occurrence of HDD aerosols in winter (Figure 7) is attributed partly to the mixing processes with the different aerosol types at lower altitudes and partly to the fact that the 4000-m air masses do not interact with the Saharan boundary layer in order for the latter to be capable to uplift and transport large amounts of dust.

[27] In premonsoon, the above situation is somewhat more confused. However, the majority of the lower air masses come from continental India and at 4000 m from northern and northwestern directions. The air masses from the different source regions lead to the formation of different aerosol types as seen in Figures 6 and 7. On several occasions the 4000-m air masses can uplift and transport HDD aerosols over Hyderabad, since they generally interact with the boundary layer over the arid/semiarid locations. Furthermore, in several cases the lower air masses come from the arid locations in northwestern India and Pakistan. In India, fires occur every year from January to May with a predominance during March and April [*Badarinath et al.*, 2007a]. The back trajectories suggest that wind patterns are dominantly northerly with continental air mass conditions prevailing over the study area during the fire season. This leads to enhanced aerosol loading with increased concentrations of BC [*Badarinath et al.*, 2007a] and fine-mode aerosols, thus increasing the α values over Hyderabad. The highly industrialized and urbanized IGP can produce anthropogenic fine particles that may be transported over long distances before they settle down due to gravity. *Niranjan et al.* [2007] have shown the presence of high-

altitude aerosol layers above the boundary layer, at a height between 1.5 to 5 km, at Visakhaptnam located on the east coast of India near to Hyderabad, during the period March–May 2005; they indicated an increase in AOD with no signs of proportional increase in the surface aerosol mass concentration. The air mass trajectories during premonsoon and early monsoon are in close agreement with those observed over New Delhi in the same months, March–June 2006 [*Pandithurai et al.*, 2008].

[28] In the monsoon period, the air circulation pattern is quite characteristic driven by the summer monsoons. Thus, although the boundary layer wind flow (at 500 and 1500 m) is clearly southwesterly, transport of dust aerosols from distinct regions of west Asia (Arabian Peninsula, Iran and Pakistan) occurs at high altitudes (4000 m). The marine and/or desert source regions of air masses in the monsoon period have an evidence of lower α values (Figures 3 and 5) and an occurrence of HDD aerosols (Figure 7). *Sagar et al.* [2004] found that in northern India the air masses shift from southerly to westerly in the period of winter-spring/summer, when the winds arrive from the vast arid regions of northwest India and others located farther to its west. This change in the air mass type was obviously mostly responsible for the rapid buildup in the AOD after March, as the arid air mass is known to transport large amounts of desert/mineral aerosols from the west Asian and Indian deserts. Finally, in the transition season of postmonsoon, the air mass trajectories exhibit a rather confused pattern, as in premonsoon, where aerosols from different origins can be present in the vertical. The main difference from the premonsoon period is the high-frequency occurrence of upper air mass from marine directions, probably responsible for the more transparent atmospheric conditions. Within the boundary layer, the air masses are mainly originating from IGP, capable to transport anthropogenic pollution and biomass burning aerosols in certain cases, for example, during Diwali festival [*Badarinath et al.*, 2009].

4.4. Optical Properties of the Different Aerosol Types

[29] In this section, the optical properties of the aerosol types are further investigated. Figure 10 shows the relative (%) frequency of occurrence for positive and negative a_2 values as a function of month. The existence of positive (negative) curvature indicates a significant contribution by coarse- (fine-) mode aerosols in the size distribution [*Eck et al.*, 1999; *Schuster et al.*, 2006]. It is shown that the negative a_2 values are predominant in the period January to April, and the positive a_2 in the rest of the year. Comparing Figure 10 with Figure 8, it is concluded that in months with significant occurrence of HUI aerosols the curvature is negative, while in months with significant fraction of MI or HDD aerosols the curvature is positive. In the first period (January–April) the comparison of Figures 10 and 8 reveals that the majority of the MT aerosols exhibit negative curvature, while in the second period (May–December) positive. This can further discriminate the initial origin of this mixed "undetermined" aerosol type. Gas-to-particle conversion, followed by coagulation and direct emission of aerosols in the accumulation mode must be the main processes explaining production of the HUI aerosols. This consists of the presence of a dense motorized traffic within Hyderabad that releases very fine
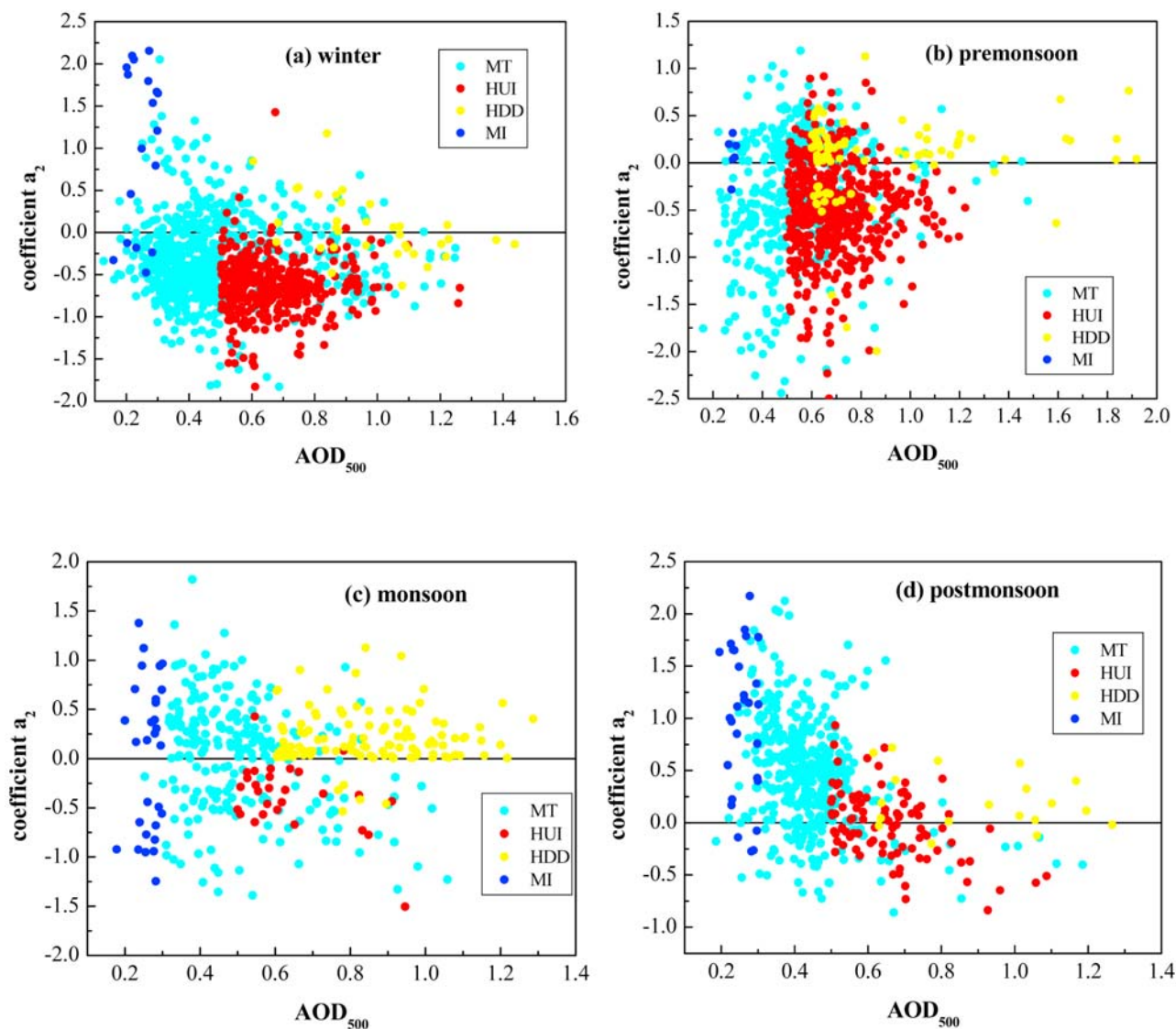
Figure 11. Seasonal correlations between coefficient a_2 and AOD_{500} for each aerosol type over Hyderabad for (a) winter, (b) premonsoon, (c) monsoon, and (d) postmonsoon.

particles found in the accumulation mode [*Badarinath et al.*, 2007a]. Indeed, the biomass burning is known to release particles in the accumulation mode but also coarser particles resulting from the condensation of organic compounds [*Reid et al.*, 1999]. The negative curvature is much greater for aged fine-mode aerosols due to particle growth by coagulation [*Eck et al.*, 2003]. This highlights why Ångström exponent alone does not give all the information for the determination of the fine/coarse mode relative contributions.

[30] Figure 11 shows the scatterplots of the coefficient a_2 (curvature in the polynomial fit) against AOD_{500} for the four aerosol types depending on season. The correlation between a_2 and AOD_{500} provides information on the atmospheric conditions under which α is independent from wavelength, so the spectral variation of AOD can be accurately described by the simple Ångström formula

(equation (1)). The data lying on or near the $a_2 = 0$ line correspond to the monomodal Junge size distribution or to bimodal lognormal aerosol size distribution without curvature. Near to zero a_2 values can also be caused by a unimodal coarse-mode size distribution, i.e., dust dominated [*Eck et al.*, 1999]. Negative a_2 values (fine-mode aerosols) are depicted, unexpectedly, for the MI type and correspond to observations associated with larger errors in the a_2 retrievals caused by uncertainties in the polynomial fit (equation (3)) under low turbid conditions [*Kaskaoutis et al.*, 2006, 2007b]. Furthermore, some positive a_2 values are presented for the HUI type, thus showing that the initial fine-mode aerosols have been modified by coagulation, condensation and gas-to-particle conversion resulting in greater size and less negative or even positive a_2 values [*Schuster et al.*, 2006]. Quite different graphs are revealed in each season. In winter and postmonsoon, and partly in
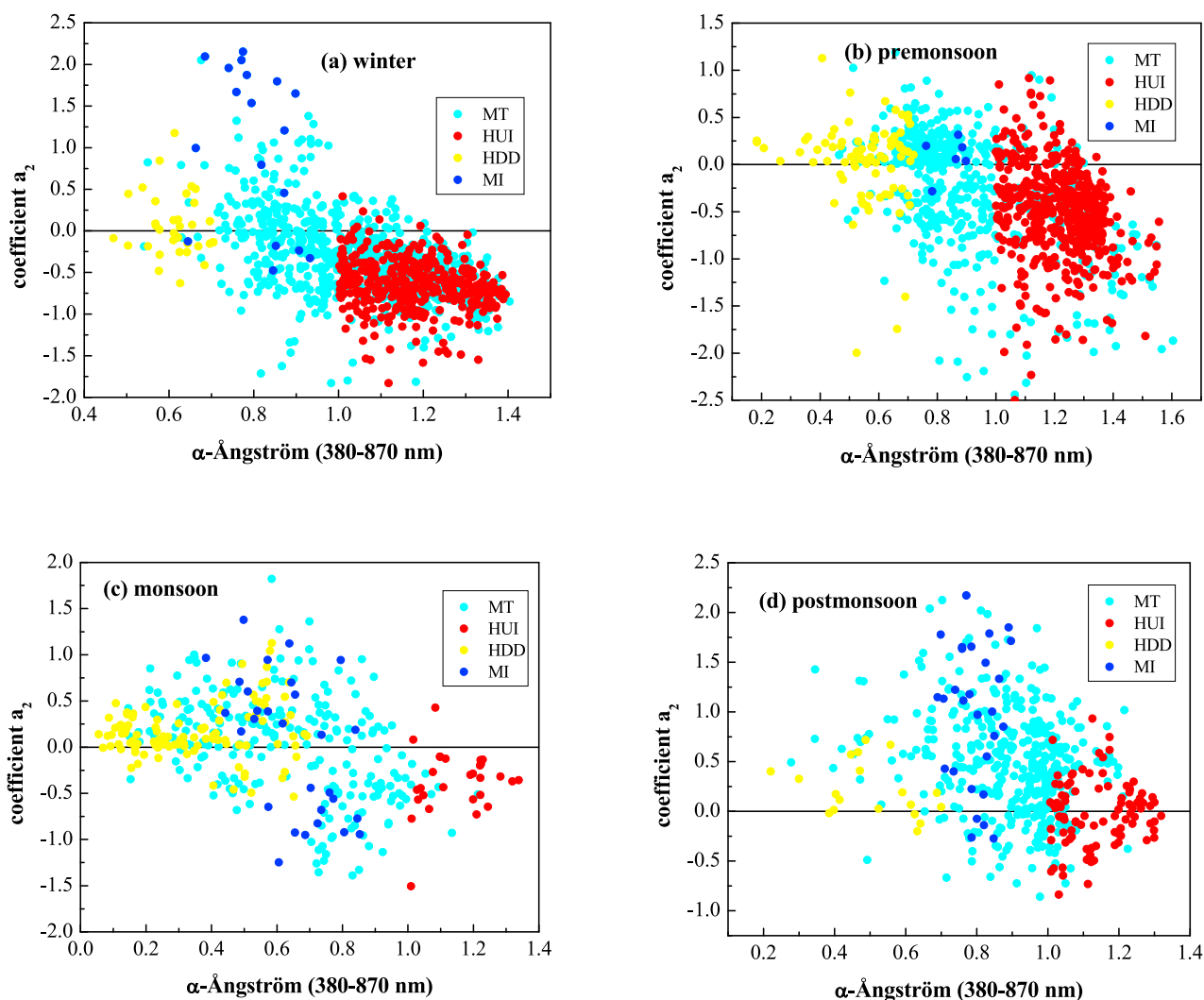
Figure 12. Same as in Figure 11 but for the correlation between a_2 and $\alpha_{380-870}$.

monsoon, a_2 presents high positive values (in the majority of the cases) for low AOD_{500}, which are reduced as AOD_{500} increases. These high positive values at low AOD are likely due to large uncertainty in computed a_2 for these cases, due to AOD uncertainty of ~ 0.03. In premonsoon, a_2 values are mostly negative for the lower AOD_{500} values. It is interesting to note the smaller fraction of positive a_2 values of MT in winter and premonsoon, highlighting the great fraction of fine-mode particles in its component; in monsoon and postmonsoon the majority of MT cases correspond to positive a_2.

[31] It is concluded that the different aerosol types are rather difficult to be distinguished based on the a_2 values, in contrast to the results in the work by *Kaskaoutis et al.* [2007b]. However, these researchers investigated the aerosol properties in different environments, where the aerosol types were clearly distinguishable, whereas the present study focuses over Hyderabad, where aerosols from different origins are present. So, except MI and some portion of HDD (at higher AODs) the other types are still unable to be discriminated unambiguously. Note also that for low

AOD_{500}, there is a wide variability in a_2 values (both positive and negative), thus implying large curvature in equation (3). It was found that in such cases the uncertainties in the polynomial fit dramatically increase as well as the errors in the a_2 values. *Kaskaoutis and Kambezidis* [2006] also found that the curvature of the polynomial fit becomes greater as the aerosol loading alters from high to low. On the other hand, coarse-mode HDD aerosols present near to zero a_2 values as the turbidity increases. This is in accordance with previous studies [e.g., *Eck et al.*, 1999; *Kaskaoutis et al.*, 2007b].

[32] Figure 12 is drawn for further aid in a clear discrimination of the aerosol types, especially of HDD, which is confined to lower $\alpha_{380-870}$ values. In general, for a specific value of $\alpha_{380-870}$, a great spread of a_2 occurs, especially for intermediate $\alpha_{380-870}$ values (0.7–0.9). This is in agreement with the findings of *Schuster et al.* [2006], who showed that different size distributions with similar α can produce large differences in curvature; they verified that the curvature alone is not enough for describing the aerosol particle size, as stated elsewhere [e.g., *Eck et al.*, 1999]. Yet,
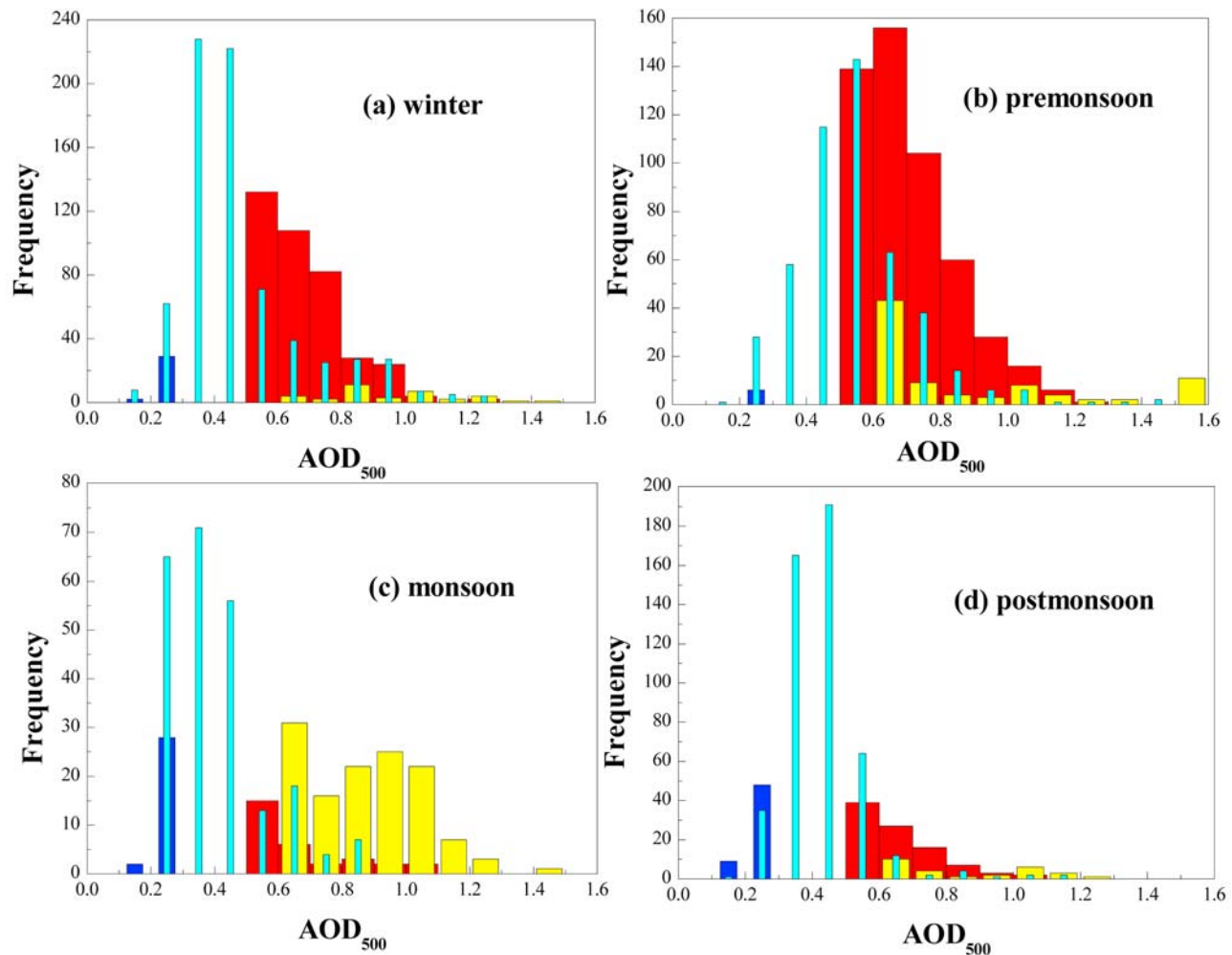
Figure 13. Number of cases of the different aerosol types based on AOD_{500} values for each season over Hyderabad. HUI in red, MI in blue, HDD in yellow, and MT in cyan for (a) winter, (b) premonsoon, (c) monsoon, and (d) postmonsoon.

it is possible to better discriminate between the different aerosol types by plotting $\alpha_{380-870}$ versus a_2. This is mainly achieved for the HDD aerosols (low $\alpha_{380-870}$ and positive or near zero a_2), but it is rather confused for identifying HUI from MT aerosols in the winter and premonsoon periods. In contrast, the HUI type is more distinguishable in the monsoon and postmonsoon periods. Despite the great differences in the $\alpha_{380-870}$ and a_2 values, there is a similarity between the graphs in each season, mainly conducted by the negative a_2 values as $\alpha_{380-870}$ increases, thus implying a general decreasing trend in their correlation. Furthermore, dominance of negative curvature was found over Visakhapatnam, India, highlighting the abundance of columnar submicron aerosols [*Madhavan et al.*, 2008]. They found that the positive curvatures dominated during the pre-rainy days, while the negative curvatures during the post-rainy days indicating that the coarse-mode aerosols had a wet deposition and the fine-mode ones acted as CCN. This was also observed at Hyderabad in the monsoon period mainly regarding the MI and the MT.

[33] Figure 13 shows the frequency distribution of AOD_{500} for the four aerosol types according to the discrim-ination criteria. Very different distribution is revealed depending on season, with the most pronounced differences to be observed in the monsoon period, when the HDD aerosols are nearly equally distributed in a wide range of AOD_{500} values (0.6–1.1). Note also the very low frequency of the other types (MT and HUI) for $AOD_{500} > 0.6$. The winter and postmonsoon distributions present some similarities, despite the lower frequency of the HUI aerosols in postmonsoon, while in premonsoon there is a clear discrimination between HUI and HDD aerosols, with the latter to dominate for $AOD_{500} > 1.1$. It was found (not presented) that all these cases correspond to dust outbreaks from the Thar Desert. During winter and postmonsoon the above situation is somewhat different. AOD_{500} maxima can then be associated either with urban pollution and mixed aerosols or, to a lesser extent, with dust particles. Large fraction of MT aerosols for $AOD_{500} > 0.5$, where also HUI and HDD aerosols can be found, is observed only in winter and premonsoon.

[34] Similarly, Figure 14 shows the frequency distribution of the aerosol types with respect to $\alpha_{380-870}$. In the scale of $\alpha_{380-870}$, HDD and MI are expected to fall in the lower end
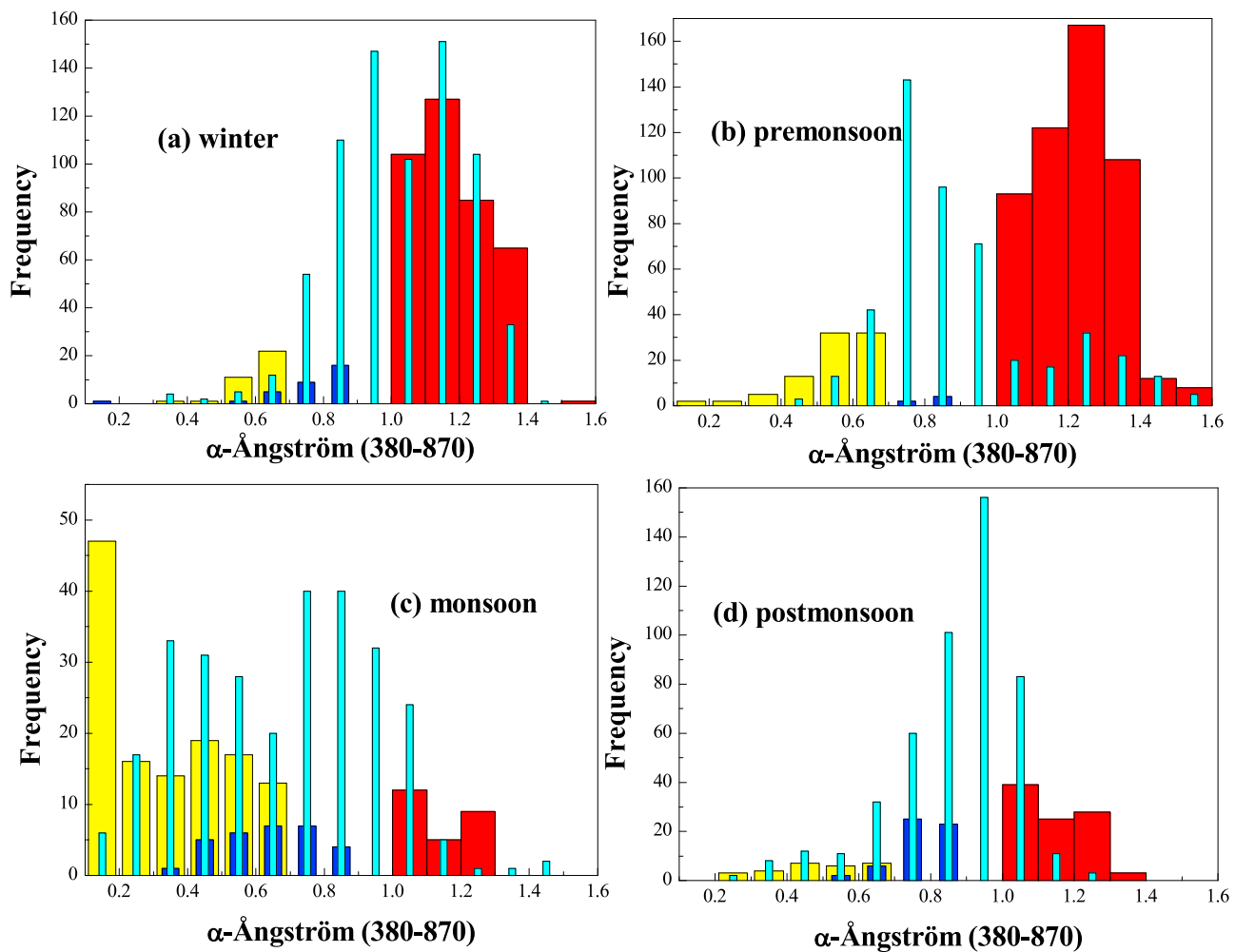
Figure 14. Same as in Figure 13 but based on $\alpha_{380-870}$ values.

of $\alpha_{380-870}$ values, since both types are characterized by coarse-mode particles. Nevertheless, it is surprising to note that the MI type is absent for $\alpha_{380-870}$ values lower than 0.4. Note that the larger possibility of observing lower $\alpha_{380-870}$ (Figure 14) in premonsoon and monsoon periods than in the rest of the year shows that the importance of the mineral component is generally greater in these seasons. This is further confirmed by examining Figure 13 showing that only the HDD aerosols are responsible for the very large $AOD_{500} > 1.1$ in these seasons. MT plays a significant role in the distribution of the $\alpha_{380-870}$ values in the winter and monsoon periods, since this is the dominant type for a wide range of $\alpha_{380-870}$ values, 0.7–1.3 for winter and 0.3–1.2 for monsoon, hindering the discrimination of the other aerosol types. On the other hand, in premonsoon, the HUI type clearly dominates for $\alpha_{380-870} > 1.0$. Therefore, it is concluded that the AOD_{500} or $\alpha_{380-870}$ values alone cannot identify any aerosol type, except of few cases, due to their similar and broad distributions.

[35] The mean seasonal values with the standard deviations of AOD_{500}, $\alpha_{380-870}$ and a_2 are given in Table 2 for each aerosol type. The AOD_{500} and $\alpha_{380-870}$ values for each aerosol type are mainly defined by the threshold values for the type identification, but it is worth noting the higher

AOD_{500} in premonsoon as well as the lower $\alpha_{380-870}$ values in monsoon independently from the aerosol type. Thus, regardless of the aerosol type the aerosol load over Hyderabad is larger in the premonsoon season directly affected by the dust exposures and/or the biomass burning. On the other hand, the AOD_{500} is lower in postmonsoon indicative of more transparent atmospheric conditions. As regards the a_2 values, the large standard deviations do not allow safe conclusions. In each season, as shown in Figures 11 and 12, they can be negative or positive. However, it is worth noting the negative mean a_2 values for the fine HUI aerosol type and the positive for the coarse HDD and MI types. The MT exhibits negative a_2 (dominance of fine-mode aerosols) in winter and premonsoon and positive (coarse-mode aerosols) in the other seasons.

5. Conclusions

[36] The Indian continent is unique with regard to aerosol sources, characteristics and their interaction with the Indian monsoon system. Seasonal variations in the aerosol optical depth and its spectral variation analyzed using a Microtops-II Sun photometer during October 2007 to September 2008 over Hyderabad were investigated. The aerosol optical

Table 2. Mean Values and Standard Deviations of AOD_{500}, $\acute{a}_{380-870}$, and a_2 for Each Aerosol Type and Season Over Hyderabad in the Period October 2007 to September 2008

Aerosol Type	Season	AOD_{500}	$\acute{a}_{380-870}$	a_2
HUI	winter	0.672 ± 0.130	1.178 ± 0.107	−0.642 ± 0.320
	premonsoon	0.701 ± 0.141	1.218 ± 0.116	−0.501 ± 0.474
	monsoon	0.639 ± 0.129	1.148 ± 0.099	−0.377 ± 0.340
	postmonsoon	0.654 ± 0.127	1.139 ± 0.161	−0.012 ± 0.329
HDD	winter	0.917 ± 0.205	0.605 ± 0.08	0.061 ± 0.377
	premonsoon	0.969 ± 0.413	0.552 ± 0.121	0.024 ± 0.450
	monsoon	0.869 ± 0.173	0.324 ± 0.185	0.202 ± 0.265
	postmonsoon	0.855 ± 0.212	0.485 ± 0.134	0.217 ± 0.274
MI	winter	0.249 ± 0.038	0.774 ± 0.140	1.048 ± 0.957
	premonsoon	0.280 ± 0.010	0.844 ± 0.057	0.084 ± 0.207
	monsoon	0.261 ± 0.248	0.638 ± 0.132	0.025 ± 0.760
	postmonsoon	0.248 ± 0.038	0.770 ± 0.074	0.981 ± 0.707
MT	winter	0.477 ± 0.194	1.026 ± 0.183	−0.295 ± 0.546
	premonsoon	0.542 ± 0.176	0.902 ± 0.224	−0.268 ± 0.624
	monsoon	0.506 ± 0.154	0.617 ± 0.240	0.011 ± 0.567
	postmonsoon	0.428 ± 0.118	0.877 ± 0.166	0.467 ± 0.524

properties exhibited large temporal variation due to the prevailing meteorology, air mass trajectories, and atmospheric conditions. The AOD_{500} presented a rather insignificant monthly variation with larger values in March–April and June (∼0.7) and lower in November and January (∼0.5). In contrast, the $\alpha_{380-870}$ exhibited a pronounced annual pattern with low values in the monsoon period and high in winter and premonsoon. The gas-to-particle reaction products of the exhausts from the industrial and urban emissions, combined with dust and sea salt during favorable wind conditions contributed to the aerosol loading in the Hyderabad urban area. The results of the study confirmed the large variability of the aerosol optical properties. They also showed that the use of detailed spectral values of AOD and Ångström exponent makes it possible to obtain the basis for characterizing some aerosol properties. Using the relationship between AOD_{500} and $\alpha_{380-870}$ three aerosol types were classified over Hyderabad in order to represent different atmospheric conditions (i.e., urban/industrial, marine influenced and desert dust aerosols). The cases, which did not belong to any of the above types, were characterized as mixed (undetermined) aerosols. The presence of each aerosol type seemed to exhibit strong temporal variability, mainly affected by the season, the long-range transport and the mixing processes in the atmospheric column. Thus, the premonsoon season presented the higher occurrence of the HUI aerosols; the HDD aerosols were mainly found in the monsoon period, while the MI conditions were identified, although rare, in the postmonsoon period. The $AOD_{500}/\alpha_{380-870}$ contour plots over Hyderabad revealed the existence of different aerosol types on certain days, months and seasons in contrast to the dominant scenario of a mixed aerosol type in the vertical over this area. To examine the effect of long-range transport, 5-days back trajectories were computed using the HYSPLIT model. The air masses in all seasons came from varying directions, mainly northwestern in the winter and premonsoon periods. In the monsoon season the lower altitude air masses

originated from AS carrying significant amount of marine aerosols over the region, while the upper atmosphere air masses came from the northwest arid and semiarid areas. This resulted in the dominance of the coarse-mode aerosols in this season. The analysis showed that the inclusion of the curvature of lnAOD with respect to lnλ did not significantly improve the aerosol type discrimination over Hyderabad. This is attributed to the mixed aerosol field over the region, since particles of different origins and sectors can be present in the atmospheric column. The dominance of positive and negative a_2 values of the MT in monsoon/postmonsoon and winter/premonsoon, respectively, suggested that the fine-mode aerosols play a much more important role in the mixed-type aerosols in winter and premonsoon and the coarse-mode particles in the rest of the year. On the other hand, the HUI presented negative a_2 values while the HDD near zero or positive, which are in agreement with other studies in the literature. The information retrieved in this way can be further used in remote sensing applications, or climatological studies, as the ground-based stations are spread all over the world and are becoming more standardized.

References

Alfaro, S. C., A. Gaudichet, J. L. Rajot, L. Gomes, M. Maillé, and H. Cachier (2003), Variability of aerosol size-resolved composition at an Indian coastal site during the Indian Ocean Experiment (Indoex) intensive field phase, *J. Geophys. Res.*, *108*(D8), 4235, doi:10.1029/2002JD002645.

Ångström, A. (1964), The parameters of atmospheric turbidity, *Tellus*, *16*, 64–75.

Anttila, T., A. Kiendler-Scharr, T. F. Mentel, and R. Tillmann (2007), Size dependent partitioning of organic material: Evidence for the formation of organic coatings on aqueous aerosols, *J. Atmos. Chem.*, *57*, 215–237, doi:10.1007/s10874-007-9067-9.

Badarinath, K. V. S., S. K. Kharol, K. Madhavi Latha, T. R. Kiran Chand, V. Krishna Prasad, A. Nirmala Jyothsna, and K. Samatha (2007a), Multi-year ground-based and satellite observations of aerosol properties over a tropical urban area in India, *Atmos. Sci. Lett.*, *8*, 7–13, doi:10.1002/asl.143.

Badarinath, K. V. S., S. K. Kharol, D. G. Kaskaoutis, and H. D. Kambezidis (2007b), Dust storm over Indian region and its impact on the ground reaching solar radiation—A case study using multi-satellite data and ground measurements, *Sci. Total Environ.*, *384*, 316–332, doi:10.1016/j.scitotenv.2007.05.031.

Badarinath, K. V. S., S. K. Kharol, D. G. Kaskaoutis, and H. D. Kambezidis (2007c), Influence of atmospheric aerosols on solar spectral irradiance in an urban area, *J. Atmos. Sol. Terr. Phys.*, *69*, 589–599, doi:10.1016/j.jastp.2006.10.010.

Badarinath, K. V. S., S. K. Kharol, V. Krishna Prasad, E. U. B. Reddi, H. D. Kambezidis, and D. G. Kaskaoutis (2008), Influence of anthropogenic activities on UV Index variations—A study over tropical urban region using ground based observations and satellite data, *J. Atmos. Chem.*, *59*, 219–236, doi:10.1007/s10874-008-9103-4.

Badarinath, K. V. S., S. K. Kharol, and A. R. Sharma (2009), Long-range transport of aerosols from agriculture crop residue burning in Indo-Gangetic Plains—A study using LIDAR, ground measurements and satellite data, *J. Atmos. Sol. Terr. Phys.*, *71*, 112–120, doi:10.1016/j.jastp.2008.09.035.

Day, D. E., and W. C. Malm (2001), Aerosol light scattering measurements as a function of relative humidity: A comparison between measurements made at three different sites, *Atmos. Environ.*, *35*, 5169–5176, doi:10.1016/S1352-2310(01)00320-X.

Devara, P. C. S., P. E. Raj, G. Pandithurai, K. K. Dani, and R. S. Maheskumar (2003), Relationship between lidar-based observations of aerosol content and monsoon precipitation over a tropical station, Pune, India, *Meteorol. Appl.*, *10*, 253–262, doi:10.1017/S1350482703003050.

Draxler, R. R., and G. D. Rolph (2003), HYSPLIT (Hybrid single-particle Lagrangian Integrated Trajectory) model, report, Air Resour. Lab., NOAA, Silver, Spring, Md. (Available at http://www.arl.noaa.gov/ready/hysplit4.html)

Dubovik, O., B. N. Holben, T. F. Eck, A. Smirnov, Y. J. Kaufman, M. D. King, D. Tanrè, and I. Slutsker (2002), Variability of absorption and optical properties of key aerosol types observed in worldwide locations, *J. Atmos. Sci.*, *59*, 590–608, doi:10.1175/1520-0469(2002)059<0590:VOAAOP>2.0.CO;2.

Eck, T. F., B. N. Holben, J. S. Reid, O. Dubovik, A. Smirnov, N. T. O'Neill, I. Slutsker, and S. Kinne (1999), Wavelength dependence of the optical depth of biomass burning, urban, and desert dust aerosols, *J. Geophys. Res.*, *104*(D24), 31,333–31,349, doi:10.1029/1999JD900923.

Eck, T. F., B. N. Holben, J. S. Reid, N. T. O'Neill, J. S. Schafer, O. Dubovik, A. Smirnov, M. A. Yamasoe, and P. Artaxo (2003), High aerosol optical depth biomass burning events: A comparison of optical properties for different source regions, *Geophys. Res. Lett.*, *30*(20), 2035, doi:10.1029/2003GL017861.

Eck, T. F., et al. (2005), Columnar aerosol optical properties at AERONET sites in central eastern Asia and aerosol transport to the tropical mid-Pacific, *J. Geophys. Res.*, *110*, D06202, doi:10.1029/2004JD005274.

El-Metwally, M., S. C. Alfaro, M. Abdel Wahab, and B. Chatenet (2008), Aerosol characteristics over urban Cairo: Seasonal variations as retrieved from Sun photometer, *J. Geophys. Res.*, *113*, D14219, doi:10.1029/2008JD009834.

Habib, G., C. Venkataraman, I. Chiapello, S. Ramachadran, O. Bopucher, and M. S. Reddy (2006), Seasonal and interannual variability in absorbing aerosols over India derived form TOMS: Relationship to regional meteorology and emissions, *Atmos. Environ.*, *40*, 1909–1921, doi:10.1016/j.atmosenv.2005.07.077.

Holben, B. N., et al. (2001), An emerging ground-based aerosol climatology: Aerosol optical depth from AERONET, *J. Geophys. Res.*, *106*(D11), 12,067–12,097, doi:10.1029/2001JD900014.

Ichoku, C., et al. (2002), Analysis of the performance characteristics of the five-channel Microtops II Sun photometer for measuring aerosol optical thickness and perceptible water vapor, *J. Geophys. Res.*, *107*(D13), 4179, doi:10.1029/2001JD001302.

Kalapureddy, M. C. R., and P. C. S. Devara (2008), Characterization of aerosols over oceanic regions around India during pre-monsoon 2006, *Atmos. Environ.*, *42*, 6816–6827, doi:10.1016/j.atmosenv.2008.05.022.

Kaskaoutis, D. G., and H. D. Kambezidis (2006), Investigation on the wavelength dependence of the aerosol optical depth in the Athens area, *Q. J. R. Meteorol. Soc.*, *132*, 2217–2234, doi:10.1256/qj.05.183.

Kaskaoutis, D. G., and H. D. Kambezidis (2008a), The role of aerosol models of the SMARTS code in predicting the spectral direct-beam irradiance in an urban area, *Renewable Energy*, *33*, 1532–1543, doi:10.1016/j.renene.2007.09.006.

Kaskaoutis, D. G., and H. D. Kambezidis (2008b), Comparison of the Ångström parameters retrieval in different spectral ranges with the use of different techniques, *Meteorol. Atmos. Phys.*, *99*, 233–246, doi:10.1007/s00703-007-0279-y.

Kaskaoutis, D. G., H. D. Kambezidis, A. D. Adamopoulos, and P. A. Kassomenos (2006), Comparison between experimental data and modeling estimates of atmospheric optical depth over Athens, Greece, *J. Atmos. Sol. Terr. Phys.*, *68*, 1167–1178, doi:10.1016/j.jastp.2006.02.011.

Kaskaoutis, D. G., H. D. Kambezidis, N. Hatzianastassiou, P. Kosmopoulos, and K. V. S. Badarinath (2007a), Aerosol climatology: On the discrimination of the aerosol types over four AERONET sites, *Atmos. Chem. Phys. Discuss.*, *7*, 6357–6411.

Kaskaoutis, D. G., H. D. Kambezidis, N. Hatzianastassiou, P. G. Kosmopoulos, and K. V. S. Badarinath (2007b), Aerosol climatology: Dependence of the Angstrom exponent on wavelength over four AERNET sites, *Atmos. Chem. Phys. Discus.*, *7*, 7347–7397.

Kaskaoutis, D. G., H. D. Kambezidis, S. K. Kharol, and K. V. S. Badarinath (2007c), Investigation on the ozone and trace gases contribution to the total optical depth in a polluted urban environment, *Atmos. Res.*, *86*, 286–296, doi:10.1016/j.atmosres.2007.06.004.

Kaskaoutis, D. G., P. Kosmopoulos, H. D. Kambezidis, and P. T. Nastos (2007d), Aerosol climatology and discrimination of different types over Athens, Greece based on MODIS data, *Atmos. Environ.*, *41*, 7315–7329, doi:10.1016/j.atmosenv.2007.05.017.

Kharol, S. K., and K. V. S. Badarinath (2006), Impact of biomass burning on aerosol properties over tropical urban region of Hyderabad, India, *Geophys. Res. Lett.*, *33*, L20801, doi:10.1029/2006GL026759.

King, M. D., and D. M. Byrne (1976), A method for inferring total ozone content from spectral variation of total optical depth obtained with a solar

radiometer, *J. Atmos. Sci.*, *33*, 2242–2251, doi:10.1175/1520-0469(1976)033<2242:AMFITO>2.0.CO;2.

Kristjànsson, J. E., T. Iversen, A. Kirkevag, Ø. Seland, and J. Debernard (2005), Response of the climate system to aerosol direct and indirect forcing: Role of cloud feedbacks, *J. Geophys. Res.*, *110*, D24206, doi:10.1029/2005JD006299.

Latha, M. K., and K. V. S. Badarinath (2005), Spectral solar attenuation due to aerosol loading over an urban area in India, *Atmos. Res.*, *75*, 257–266, doi:10.1016/j.atmosres.2005.01.002.

Latha, M. K., et al. (2004), Impact of biomass burning aerosols on UV erythema-a case study from northeast region of India, *J. Atmos. Sol. Terr. Phys.*, *66*, 981–986, doi:10.1016/j.jastp.2004.03.005.

Lau, K. M., M. K. Kim, and K. M. Kim (2006), Asian summer monsoon anomalies induced by direct forcing: The role of the Tibetan plateau, *Clim. Dyn.*, *26*, 855–864, doi:10.1007/s00382-006-0114-z.

Madhavan, B. L., K. Niranjan, V. Sreekanth, M. M. Sarin, and A. K. Sudheer (2008), Aerosol characterization during the summer monsoon period over a tropical coastal Indian station, Visakhapatnam, *J. Geophys. Res.*, *113*, D21208, doi:10.1029/2008JD010272.

McComiskey, A., S. E. Schwartz, B. Schmid, H. Guan, E. R. Lewis, P. Richiazzi, and J. A. Ogren (2008), Direct aerosol forcing: Calculation from observations and sensitivities to inputs, *J. Geophys. Res.*, *113*, D09202, doi:10.1029/2007JD009170.

Moorthy, K. K., et al. (1999), Aerosol climatology over India: 1. ISRO GBR MWR network and database, *ISRO GBR SR-03-99*, Indian Space Res. Organ, Bangalore, India.

Morgan, M. G., P. J. Adams, and D. W. Keith (2006), Elicitation of expert judgments of aerosol forcing, *Clim. Change*, *75*, 195–214, doi:10.1007/s10584-005-9025-y.

Morys, M., F. M. Mims III, S. Hagerup, S. E. Anderson, A. Baker, J. Kia, and T. Walkup (2001), Design, calibration, and performance of MICROTOPS II handheld ozone monitor and Sun photometer, *J. Geophys. Res.*, *106*(D13), 14,573–14,582, doi:10.1029/2001JD900103.

Naseema Beegum, S., et al. (2009), Spatial distribution of aerosol black carbon over India during pre-monsoon season, *Atmos. Environ.*, *43*, 1071–1078, doi:10.1016/j.atmosenv.2008.11.042.

Niranjan, K., B. L. Madhavan, and V. Sreekanth (2007), Micro pulse lidar observation of high-altitude aerosol layers at Visakhaptnam located on the east coast of India, *Geophys. Res. Lett.*, *34*, L03815, doi:10.1029/2006GL028199.

Novakov, T., M. O. Andreae, R. Gabriel, T. W. Kirchstetter, O. L. Mayol-Bracero, and V. Ramanathan (2000), Origin of carbonaceous aerosols over the tropical Indian Ocean: Biomass burning or fossil fuels?, *Geophys. Res. Lett.*, *27*(24), 4061–4064, doi:10.1029/2000GL011759.

Ogunjobi, K. O., Z. He, and C. Simmer (2008), Spectral aerosol optical properties from AERONET Sun-photometric measurements over West Africa, *Atmos. Res.*, *88*, 89–107, doi:10.1016/j.atmosres.2007.10.004.

Pace, G., A. di Sarra, D. Meloni, S. Piacentino, and P. Chamard (2006), Aerosol optical properties at Lampeduca (central Mediterranean). 1. Influence of transport and identification of different aerosol types, *Atmos. Chem. Phys.*, *6*, 697–713.

Pandithurai, G., R. T. Pinker, P. C. S. Devara, T. Takamura, and K. K. Dani (2007), Seasonal asymmetry in diurnal variation of aerosol optical characteristics over Pune, western India, *J. Geophys. Res.*, *112*, D08208, doi:10.1029/2006JD007803.

Pandithurai, G., S. Dipu, K. K. Dani, S. Tiwari, D. S. Bisht, P. C. S. Devara, and R. T. Pinker (2008), Aerosol radiative forcing during dust events over New Delhi, India, *J. Geophys. Res.*, *113*, D13209, doi:10.1029/2008JD009804.

Pedrós, R., J. A. Martinez-Lozano, M. P. Utrillas, J. L. Gomez-Amo, and F. Tena (2003), Column-integrated aerosol, optical properties from ground-based spectroradiometer measurements at Barrax (Spain) during the Digital Airborne Imaging Spectrometer Experiment (DAISEX) campaigns, *J. Geophys. Res.*, *108*(D18), 4571, doi:10.1029/2002JD003331.

Porter, J. N., M. Miller, C. Pietras, and C. Motell (2001), Ship based Sun photometer measurements using Microtops Sun photometer, *J. Atmos. Oceanic Technol.*, *18*, 765–774, doi:10.1175/1520-0426(2001)018<0765:SBSPMU>2.0.CO;2.

Ramachandran, S. (2004), Spectral aerosol optical characteristics during the Northeast monsoon over the Arabian Sea and the tropical Indian Ocean: 2. Ångström parameters and anthropogenic influence, *J. Geophys. Res.*, *109*, D19208, doi:10.1029/2003JD004483.

Ramachandran, S. (2007), Aerosol optical depth and fine mode fraction variations deduced from Moderate Resolution Imaging Spectroradiometer (MODIS) over four urban areas in India, *J. Geophys. Res.*, *112*, D16207, doi:10.1029/2007JD008500.

Ramanathan, V., et al. (2001), Indian Ocean Experiment: An integrated analysis of the climate and the great Indo-Asian haze, *J. Geophys. Res.*, *106*(D22), 28,371–28,398, doi:10.1029/2001JD900133.

Reid, J. S., T. F. Eck, Ṣ. A. Christopher, P. V. Hobbs, and B. N. Holben (1999), Use of the Angstrom exponent to estimate the variability of optical and physical properties of aging smoke particles in Brazil, *J. Geophys. Res.*, *104*(D22), 27,473–27,489, doi:10.1029/1999JD900833.

Remer, L. A., and Y. J. Kaufman (2006), Aerosol direct radiative effect at the top of the atmosphere over cloud free ocean derived from four years of MODIS data, *Atmos. Chem. Phys.*, *6*, 237–253.

Roberts, G. C., P. Artaxo, J. Zhou, E. Swietlicki, and M. O. Andreae (2002), Sensitivity of CCN spectra on chemical and physical properties of aerosol: A case study from the Amazon Basin, *J. Geophys. Res.*, *107*(D20), 8070, doi:10.1029/2001JD000583.

Russell, P. B., et al. (1993), Pinatubo and pre-Pinatubo optical depth spectra: Mauna Loa measurements, comparisons, inferred particle size distribution, radiative effects and relationships to Lidar data, *J. Geophys. Res.*, *98*(D12), 22,969–22,985, doi:10.1029/93JD02308.

Sagar, R., B. Kumar, U. C. Dumka, K. K. Moorthy, and P. Pant (2004), Characteristics of aerosol spectral optical depths over Monora Peak: A high altitude station in the central Himalayas, *J. Geophys. Res.*, *109*, D06207, doi:10.1029/2003JD003954.

Satheesh, S. K., V. Ramanathan, B. N. Holben, K. K. Moorthy, N. G. Loeb, H. Maring, J. M. Prospero, and D. Savoie (2002), Chemical, microphysical, and radiative effects of Indian Ocean aerosols, *J. Geophys. Res.*, *107*(D23), 4725, doi:10.1029/2002JD002463.

Satheesh, S. K., K. K. Moorthy, Y. J. Kaufman, and T. Takemura (2006), Aerosol optical depth, physical properties and radiative forcing over the Arabian Sea, *Meteorol. Atmos. Phys.*, *91*, 45–62, doi:10.1007/s00703-004-0097-4.

Schuster, G. L., O. Dubovik, and B. N. Holben (2006), Angstrom exponent and bimodal aerosol size distributions, *J. Geophys. Res.*, *111*, D07207, doi:10.1029/2005JD006328.

Smirnov, A., B. N. Holben, T. F. Eck, O. Dubovic, and I. Slutsker (2000), Cloud-screening and quality control algorithms for the AERONET database, *Remote Sens. Environ.*, *73*, 337–349, doi:10.1016/S0034-4257(00)00109-7.

Smirnov, A., B. N. Holben, O. Dubovic, N. T. O'Neil, T. F. Eck, D. L. Westphal, A. K. Goroth, C. Pietras, and I. Slutsker (2002), Atmospheric aerosol optical properties in the Persian Gulf, *J. Atmos. Sci.*, *59*, 620–634, doi:10.1175/1520-0469(2002)059<0620:AAOPIT>2.0.CO;2.

Tafuro, A. M., S. Kinne, F. De Tomasi, and M. R. Perrone (2007), Annual cycle of aerosol direct radiative effect over southeast Italy and sensitivity studies, *J. Geophys. Res.*, *112*, D20202, doi:10.1029/2006JD008265.

Tripathi, S. N., S. Dey, A. Chandel, S. Srivastava, R. P. Singh, and B. N. Holben (2005), Comparison of MODIS and AERONET derived aerosol optical depth over the Ganga Basin, India, *Ann. Geophys.*, *23*, 1093–1101.

Wang, J., and S. A. Christopher (2003), Intercomparison between satellite-derived aerosol optical thickness and $PM_{2.5}$ mass: Implications for air quality studies, *Geophys. Res. Lett.*, *30*(21), 2095, doi:10.1029/2003GL018174.

Xin, J., S. Wang, Y. Wang, J. Yuan, W. Zhang, and Y. Sun (2005), Optical properties and size distribution of dust aerosols over the Tengger Desert in northern China, *Atmos. Environ.*, *39*, 5971–5978, doi:10.1016/j.atmo-senv.2005.06.027.

Yu, H., et al. (2006), A review of measurement-based assessment of aerosol direct radiative effect and forcing, *Atmos. Chem. Phys.*, *6*, 613–666.

————————————

K. V. S. Badarinath, S. Kumar Kharol, and A. Rani Sharma, Atmospheric Science Section, Oceanography Division, National Remote Sensing Centre, Department of Space, Government of India, Balanagar, Hyderabad 500 625, India. (badrinath_kvs@nrsc.gov.in; shaileshan2000@yahoo.co.in)

H. D. Kambezidis and D. G. Kaskaoutis, Atmospheric Research Team, Institute for Environmental Research and Sustainable Development, National Observatory of Athens, Lofos Nymphon, P.O. Box 20048, GR-11810 Athens, Greece.